White Rose Research Online

eprints@whiterose.ac.uk
https://eprints.whiterose.ac.uk
Universities of Leeds, Sheffield and York

Deposited via The University of Leeds.

White Rose Research Online URL for this paper:
https://eprints.whiterose.ac.uk/id/eprint/167826/

Version: Accepted Version

Article:
Medici, G, Baják, P, West, LJ et al. (2021) DOC and nitrate fluxes from farmland; impact on a dolostone aquifer KCZ. Journal of Hydrology, 595. 125658. ISSN: 0022-1694

https://doi.org/10.1016/j.jhydrol.2020.125658

© 2020, Elsevier. This manuscript version is made available under the CC-BY-NC-ND 4.0 license http://creativecommons.org/licenses/by-nc-nd/4.0/.

Reuse
This article is distributed under the terms of the Creative Commons Attribution-NonCommercial-NoDerivs (CC BY-NC-ND) licence. This licence only allows you to download this work and share it with others as long as you credit the authors, but you can't change the article in any way or use it commercially. More information and the full terms of the licence here: https://creativecommons.org/licenses/

Takedown
If you consider content in White Rose Research Online to be in breach of UK law, please notify us by emailing eprints@whiterose.ac.uk including the URL of the record and the reason for the withdrawal request.

UNIVERSITY OF LEEDS
University of Sheffield
UNIVERSITY of York

DOC and Nitrate fluxes from farmland; impact on a dolostone aquifer KCZ

Medici G[1]*, Baják P[2], West LJ[3], Chapman PJ[4], Banwart SA[3]

[1] G[360] Institute of Groundwater Research, University of Guelph, Stone Road, Guelph, Ontario, N1G 2W1, Canada

[2] József and Erzsébet Tóth Endowed Hydrogeology Chair, Institute of Geography and *Earth Sciences,* Eötvös Loránd University, Pázmány Péter Sétány, Budapest-1117, Hungary

[3] School of Earth and Environment, University of Leeds, Woodhouse Lane, Leeds, W Yorkshire LS2 9JT, UK

[4] Water@leeds, School of Geography, University of Leeds, Woodhouse Lane, Leeds, W Yorkshire LS2 9JT, UK

* Corresponding author: giacomo.medici@g360group.org

Abstract

DOC and nitrate in farmland represent key chemical species that determine the water quality in the Karst Critical Zone (KCZ). The work reported here focuses on quantifying fluxes of these species in an experimental farm site (University of Leeds Farm, UK) overlying a dolomitic karst aquifer of Permian age. In this research, the Transect Method was applied for the first time to farmland by combining hydrochemical data from soil and groundwater for computation of mass fluxes. The Transect Method, developed for management of industrially contaminated sites, was applied to a farm source due to the presence of localised contamination from application of pig slurry.

Required inputs for our approach include concentrations of nitrate and DOC in soil water and groundwater, net recharge flux (here derived from a MODFLOW-2005 model) and local hydraulic gradient and conductivity measurements. Key outputs are fluxes and downstream groundwater concentrations of DOC and nitrate. Downstream concentrations were validated against direct groundwater measurements, demonstrating the veracity of the approach. The approach shows that the localised contamination has a significant impact on both concentrations of nitrate and DOC in groundwater, although the DOC impact is greater, because the upstream land uses also produce nitrate as a result of agricultural practices that are widespread in the region.

The results of the study also constrain the zone vulnerable to contamination to the upper ~40 m below the ground surface. Future modelling efforts on solute contaminant transport should focus on this shallow vulnerability zone (0-40 mBGL) and the Transect Method applied in this work can be used to define boundary conditions.

Hence, following this research, we envisage to export a generic approach that combines physical flow parameters and hydrochemical analyses for computation of subsurface mass fluxes using the Transect Method, to identify the degree of impact of specific point sources and to support conceptualization and modelling of contaminant transport in the KCZ of farm areas.

Keywords Karst Critical Zone, Farmland, DOC, Nitrate, Mass Flux, Contaminant Transport

1. Introduction

The Critical Zone is the thin surface layer that extends from the top of the vegetation to the bottom of active groundwater circulation driven by meteorological recharge and supplies humans with most life-sustaining resources (Banwart et al. 2011, 2017; Anderson et al.

2014; Brantley et al. 2017; Keller 2019). Karst aquifers of carbonate origin represent a source of drinking water that supplies a quarter of the world's population (Ford and Williams 1989; Hartman et al. 2014). This category of fractured aquifers is particularly prone to dissolution that enlarges bedding planes, fractures and faults. Consequently, karst aquifers are characterized by a high degree of hydraulic connectivity with the land surface and transport of contaminants is therefore particularly rapid (Ford and Williams 1989; Worthington et al. 2012; Goldscheider and Drew 2014; Medici et al. 2016; Borović et al. 2019; Torresan et al. 2020). The Critical Zone in karst environment is considered as the most vulnerable to contamination due to the above mentioned dissolution processes in the vadose and shallow saturated zone of carbonate aquifers (Lian et al. 2011; Kogovsek and Petric 2014; Zhang et al. 2017; Jiang et al. 2019; Jourde et al. 2018; Green et al. 2019; Sullivan et al. 2019). Stress on groundwater resources of the KCZ has increased in recent decades in agricultural areas in terms of (i) quantity due to excessive abstraction of groundwater for irrigation, and (ii) water quality due to pollution from agricultural practices (Maheler and Massei 2007; Bicalho et al. 2011; Huebsch et al. 2013; Goldscheider and Drew 2014; Hartman et al. 2014). The research presented in this paper focuses on the second aspect of interest to the KCZ international community that is represented by protection of water resources from contamination.

Applications of N-fertilizer and manure have increased crop yields while also increasing nitrate concentrations in ground and surface water. For example, Defra (2002) estimated that between 70 and 80% of nitrate in English surface and groundwater derives from agricultural activities. Other sources of nitrate include atmospheric deposition, discharge from septic tanks and leaking sewers, the spreading of sewage sludge to land and seepage from landfills (Wakida and Lerner, 2005; Fezzi et al. 2010; Hutchins 2012). Elevated nitrate in groundwater has implications for human health. Therefore, quantification of nitrate fluxes in the unsaturated zone and groundwater across agricultural

78 areas is a key element of managing water resources. However, few studies have
79 effectively integrated water quality data and hydrogeological information to estimate fluxes
80 of nitrate, or other pollutants, from agricultural soils to the unsaturated zone and shallow
81 groundwater (Liao et al. 2012; Green et al. 2018). To integrate these research areas
82 dedicated to nitrate pollution, we present a baseline hydro-chemical analysis of soil and
83 groundwater water which we use to compute both DOC and nitrate mass fluxes for the
84 University of Leeds (UoL) Farm, UK (Figs. 1a-c).
85 The amount of nitrate available for leaching from the soil is related to the amount, timing
86 and method of application of inorganic fertilizers, slurry and/or farmyard manure to
87 agricultural land (Foster 1976; Sieling et al. 1997; Lord et al. 1999; Williams et al. 2000;
88 Wang et al. 2016). Furthermore, the rate of nitrate leaching through the soil is controlled by
89 texture, with sandy soils allowing more leaching through larger better connected pore
90 spaces than clay rich soils (Goss et al. 1998). The fraction of applied nitrogen that is
91 actually leached to groundwater (‘‘leaching fraction’’) from the soil zone is a key parameter
92 linking nitrogen applications to groundwater nitrate concentrations and typically ranges
93 between 5 and 50% (Liao et al. 2012; Green et al. 2018). Nitrate leaching will also depend
94 on the extent of denitrification within the soil zone, which is function of the nitrate and DOC
95 concentrations, fluid temperature, pH and alkalinity and is therefore strongly dependant on
96 the characteristics of the study site (Panno et al. 2001; Rivett et al. 2008; Mellander et al.
97 2012; Yang et al. 2020). Denitrification in groundwater in limestone aquifers can also occur
98 (Panno et al. 2001) but is likely to be limited at our field site due to relatively low
99 temperatures, dolostone lithology and rapid fracture flow (Rivett et al., 2008; Moon et al,
100 2006). Furthermore, Siemens et al. (2003) found in their study that DOC leached from
101 agricultural soils contributed negligibly to the denitrification of nitrate in groundwater
102 because the DOC derived from the soil was not bio-available. Toxic hydrophobic organic
103 contaminants are released by pesticides and form complexes with DOC that facilitates

104 their transport through the soil to the aquifer below (Huang et al. 1998; Weber et al. 1998;
105 Wang et al. 2004, 2016, 2018). Given the role of DOC in influencing both sorption and
106 biodegradation process its importance in influencing groundwater chemistry has been
107 increasingly recognised (Allen-King et al. 2002). Hence, detection of the most vulnerable
108 aquifer zone to infiltration and transport of both DOC and nitrate is included in this
109 research.

110 To date, the Critical Zone scientific network has primary focused on weathering processes
111 and the geochemical properties of soil and vadose zone using laboratory experimental and
112 modelling approaches (e.g., Emblanch et al. 2003; Falcone et al. 2008; Peyraube et al.
113 2012, 2013; Dong et al. 2018; Lerch et al. 2018; Zhou et al. 2019; Tremosa et al. 2020).
114 Consequently, there is need for more field scale monitoring and hydraulic testing to
115 characterize the unsaturated and saturated zone as recently highlighted by Critical Zone
116 scientists Kuntz et al. (2011) and Jourde et al. (2018), and shown in this work.

117 Previous hydrogeological research at the UoL Farm consists of multi-level slug tests
118 (Medici et al. 2019a), pumping tests (Allen et al. 1997) and development of a regional
119 scale steady state MODFLOW-2005 groundwater flow model (Medici et al. 2019b) of the
120 local dolostone aquifer of Permian age. The three formations (Cadeby, Edlington and
121 Brotherton illustrated in Figure 1c) of the Mangnesian Limestone Group represents
122 separate layers in the model. This groundwater flow model accounts for turbulent flow by
123 inserting the Conduit Flow Process Type-1 (*sensu* Hill et al. 2010) developed by the USGS
124 for karst systems in correspondence of streams and normal faults. Indeed, transmissivities
125 from pumping tests in correspondence of streams and faults is one order of magnitude
126 higher than the host rock due to the presence of karst conduits 0.10-0.20 m large of
127 approximate pipe shape (Medici et al. 2019b). This modelling research has produced
128 calibrated recharge and hydraulic conductivity values that represent inputs for the workflow
129 presented here (Medici et al. 2019a, b).

Nitrate and DOC represent two chemical species, which are considered diagnostic of water quality pollution in karst environments in areas of the world characterized by intense agricultural activities (Ryan and Meiman 1996; Lastennet and Mudry 1997; Goldscheider and Drew 2014). The aim of this research is therefore to show how the combination of groundwater hydrological fluxes with soil water chemistry, baseline groundwater hydrochemistry and monitoring supports reliable computation of DOC and nitrate fluxes from specific agricultural activities which represent point source inputs, developing a method that can be applied in other farmlands overlying KCZs. The specific research objectives were: (i) determine baseline hydrochemical analysis of soil, spring and stream water and groundwater in the KCZ under the UoL Farm, (ii) detect depth of penetration of farm-derived nitrate and DOC in the sub-surface, and (iii) compute and validate nitrate and DOC mass fluxes and downstream concentrations in groundwater in an area of farming activity.

2 Field site

2.1 Bedrock geology

The experimental site of the UoL Farm (see Figs. 1a-d, 2) is located in Yorkshire (NE England, UK) between the cities of Leeds and York. Here, the Magnesian Limestone Group represents the major aquifer and the bedrock lithology. This geological group of Lower Permian age is comprised of dolomitic limestone, dolostone, halite and gypsum rocks derived from shallow water sedimentation at the margins of the Zechstein Basin (Fig. 1a; Aldrick 1978; Smith et al. 1986). In NE England, the stratigraphic succession of the Magnesian Limestone Group is typically 120 m thick (Cooper and Lawley 2007). This geological group is formally sub-divided into three different formations: the Cadeby, Edlington and Brotherton formations (Fig. 2a; Smith et al. 1986). The Cadeby Formation that represents the focus of this research is characterized, with the exception of the basal

156 5 meters of marls, by thinly bedded dolostone showing ooids, peloids, corals and bivalves
157 (Tucker 1991; Mawson and Tucker 2009). The Brotherton Formation above represents the
158 uppermost part of the Magnesian Limestone Group in Yorkshire and is characterized by
159 thinly bedded dolomitic limestones with ooids, algae and bivalves. However, the Edlington
160 Formation is characterized by both halite and gypsum (Smith et al., 1986).
161 Higher dolomitisation characterizes the Cadeby Formation (54% $CaCO_3$; 46% $MgCO_3$) that
162 represents the focus of this study. In contrast, the dolomitic limestone of the Brotherton
163 Formation is more abundant in calcite (65% $CaCO_3$; 35% $MgCO_3$), hence more prone to
164 dissolution and permeability development (Allen et al. 1997; Lott and Cooper 2005). In NE
165 England around the area of study (Figs. 1c, 2a), the tectonic structures which characterize
166 the UK Magnesian Limestone Group are represented by normal faults and non-
167 stratabound joints (*sensu* Odling et al. 1999). Outcrop studies and seismic lines carried out
168 near the field site show how normal faults of Mesozoic age are mainly oriented ENE-WSW
169 (Fig. 1c, 2a). Lack of significant effects of the Cenozoic Alpine orogenesis results in the
170 gentle dip (< 5° towards E) of the Permo-Mesozoic deposits in the study area (Fig. 1c, d,
171 2a; Murphy 2000).
172 Boreholes drilled in non-faulted sections of the Cadeby Formation show high angle joints
173 (dip 50°-80°) which cross-cut the bedding parallel fractures (Medici et al. 2019a). Cavities
174 of karstic origin up to 0.6 m large were detected in correspondence of fault zones in the
175 study area (Cooper and Lawley 2007; Medici et al. 2019b). Vuggy porosity was detected at
176 the field site in cores drilled in the vadose zone (Murphy 2000; Murphy and Cordingly
177 2010). Discontinuity surveys indicate 0.7 and 0.3 mm average mechanical apertures for
178 sub-vertical joints and bedding plane, respectively (Medici et al. 2019b). Note that,
179 availability of a seismic survey, cores and quarry outcrops allows good spatial constraints
180 on geological formations and presence of faults in the UoL Farm area (Fig. 2a; Cooper and
181 Lawley 2007).

182

183 *2.2 Land use and hydrogeology*

184 The aquifer-unit of the Cadeby Formation is unconfined at the UoL Farm site due to the
185 presence of only ~1 m thick Quaternary cover. The soil above the dolostone is a well-
186 drained, loamy, calcareous brown earth type from the Aberford series of Calcaric Edoleptic
187 Cambisols, and ranges in depth from 0.5 to 0.9 m (Holden et al. 2019). This soil type
188 occurs extensively across the UK on gently sloping Permian and Jurassic Limestone and
189 is mainly used for arable farming. The farm is comprised of 294 ha, the majority (264 ha)
190 of which is arable with the remainder under grass. The arable fields have been in
191 continuous cultivation and cropping since 1994 using a rotation of winter wheat (x2), spring
192 or winter barley and oilseed rape, with the periodic inclusion of vining peas or potatoes.
193 The grass fields are used for sheep grazing and some are cut for silage up to twice per
194 year. Approximately 150 kg N ha^{-1} is applied to the cereal crops as fertiliser in spring with
195 an additional 40 kg N ha^{-1} applied in the autumn as pig slurry after harvest. The grass
196 fields receive 100-130 kg N ha^{-1} as fertiliser in spring and an additional 50 kg N ha^{-1} from
197 pig slurry after silage harvest in June (Holden et al. 2019; Ward 2020). The UoL Farm is
198 distinct from the immediate surrounding agricultural land in that it applies pig slurry to both
199 the arable fields and pasture fields as it has indoor and outdoor herds of pigs.
200 Below the soil, groundwater flow occurs in the saturated zone of the Cadeby Formation.
201 This dolostone aquifer of Permian age is characterized by interquartile interval ranges for
202 intergranular hydraulic conductivity and porosity which are 2.9×10^{-4} to 0.9×10^{-3} m/day and
203 8.5 to 18.7%, respectively (Allen et al. 1997). Flow occurs essentially in correspondence of
204 fractures, i.e. evidenced by the large difference between permeability from pumping and
205 core plug tests ($K_{well\text{-}test}/K_{core\text{-}plug}$ ~ 10^4; see Fig. 3). Groundwater flow is more vigorous in
206 correspondence of normal faults and here the bedrock is heavily karstified and fault traces
207 are characterized by alignment of springs and streams that are located 3-4 km away from

the study site (Fig. 1c). Fluid temperature and electrical conductivity are in the range of 9° - 10° and 80 -110 mS/m respectively according to the probes installed in the boreholes of the UoL Farm (Medici et al. 2019a). Flow rate ranges of springs and streams are 0.1 - 1 m^3/s and 0.1 - 4 m^3/s , respectively (Aldrick 1978).

Slug tests in the Cadeby Formation conducted at the UoL site show hydraulic conductivities ranging from 0.07 to 2.89 m/day (Medici et al. 2019a). Notably, higher values of hydraulic conductivities (K=0.83-2.89 m/day) from these tests characterize the first ~15 m below the water table (Medici et al. 2019a). Pumping tests indicate hydraulic conductivities ranging from 0.2 to 10 m/day with median values of 1.3 m/day across un-faulted areas for the Cadeby Formation of NE Yorkshire. The calibrated hydraulic conductivity for the Cadeby Formation from a MODFLOW-2005 steady state model for this area is 1.75 m/day (i.e. a similar value to those from pumping and shallow slug tests, see Fig. 3). Hence, the permeability of this dolostone aquifer primary comes from enhancement of fracture hydraulic aperture in first ~15 m below the water table (Medici et al. 2019a, b). At such depths, hydraulic apertures (0.33-0.43 mm) have been computed applying the cubic law combining slug and fluid and televiewer logging at the study site (Medici et al. 2019a). This information on enhancement of hydraulic conductivity due to karstification has been incorporated in the MODFLOW-2005 flow model of the study site (Medici et al. 2019a, b). Maximum fluctuations of the water table are typically 3.5 m during the hydrological year. As a consequence of the relatively small fluctuation of the water table, the model exclusively simulates steady state flow conditions and a constant rainfall recharge rate corresponding to the annual average of 0.134 m/year was applied.

3. Material and Methods

3.1 Hydrochemistry

3.1.1 Water sampling

Water samples were collected from a variety of different sources, in order to characterize the hydrochemistry of the study site at and around the UoL Farm (field areas shown in Figs. 1b-d, 2a, b). These sources include; soil (n=102), boreholes (n=123, maximum depth 112m), springs (n=29) and streams (n=22) (Fig. 1a-d). However, it should be noted that no springs or streams occur within the UoL research farm.

Soil water was sampled from both arable (n=50) and pasture (n=52) fields every two weeks between January and October 2017 using a 5-cm MacroRhizo (Eijkelkamp, Holland) soil moisture sampler (0.02 m diameter, 0.09 m length) resulting in a total of 102 samples. Six fields were studied; three fields were arable and three were improved permanent grassland (location of these fields A1-3 and P1-3 are shown in Figure 2b). Soil water samples were collected at the depth intervals of 0.05-0.10 m and 0.35-0.40 m.

The boreholes are divided into two groups that penetrate the Cadeby Formation to different depths. Group 1 are boreholes installed by the UoL at the Farm site (BH1, BH2 and BH3, see Fig. 1d and 2b) where the water table is between 10 to 15 m below ground level (BGL). Group 1 boreholes are characterized by a diameter 0.20 m large at the UoL Farm. This group of boreholes were screened with 2.3 - 3 m long intervals between 8 and 40 mBGL and were sampled 6 times from October 2017 to September 2018. Thus, groundwater samples were collected at multiple depths in each of the UoL boreholes. Group 2 are boreholes sampled by the Environment Agency of England (EA, see Fig. 1d) in the vicinity of the UoL Farm; these are typically deeper and are screened within the depth interval 15-112 mBGL and are characterized by diameters ranging from 0.15 and 0.60 m. In addition, the EA also collected water samples from springs and streams near the farm (Fig 1d). The samples from springs, streams and Group 2 boreholes were collected two times per year by EA staff between 2006 to 2018.

3.1.2 Chemical analysis

Hydrochemical analysis of cations (Na^+, Mg^{2+}, K^+, Ca^{2+}, Mn^{2+}, Fe^{2+}, Al^{3+}), anions (Cl^-, SO_4^-, NO_3^-, HCO_3-) and DOC have been undertaken in streams, springs and groundwater within the dolostone of the Cadeby Formation to characterize the Critical Zone of the UoL Farm area (field area shown in Figures 1b, d; 2a, b). Soil water samples were analysed using a Mettler Toledo S20 pH meter, Horiba LAQUAtwin conductivity meter, and a Skalar San ++ continuous flow analyser for NO_3^- concentrations. Dissolved organic and inorganic carbon (DOC and DIC, respectively) concentrations were determined using an Analytik Jena Multi N/C 2100C combustion analyser.

The temperature, electrical conductivity and pH of all groundwater, spring, and stream samples was measured using a 6PFCE Ultrameter 2 (Myron L Company). Groundwater alkalinity was measured by titration in the field. Calibration of probes was carried out at the beginning of each working day and maintenance of calibration was assessed prior to each measurement. All groundwater samples were filtered through a 0.25 µm pore membrane into a 50 ml bottle in the field using a syringe; a 10% nitric acid was added to those 50 mL bottles intended for cation analyses. All groundwater, spring and stream water samples were stored at 4° C in the fridge prior to laboratory analyses (following Piper 1953). Major anions (Cl^-, SO_4^{2-}, NO_3^-) and cations (Na^+, Mg^{2+}, K^+, Ca^{2+}, Mn^{2+}, Fe^{2+}, Al^{3+}) were determined using an ICS0 ion chromatographer and ICP, respectively. Charge balance errors were calculated and ranged from 0.1 up to 4.5%, which suggests good quality data.

Dissolved organic carbon (DOC) concentrations in all groundwater samples was calculated from the difference between total dissolved carbon (DC) and dissolved inorganic carbon (DIC), which was measured by a Multi N/C Analyser. A comparison was made between the dissolved inorganic carbon concentration from the laboratory analysis and that derived from the alkalinity titration in the field; concentrations were very similar (+/- 2.5% discrepancy) indicating good sample preservation.

285 *3.2 Calculation of nitrate and DOC mass fluxes*

286 The Transect Method (*sensu* Goltz et al. 2007) was applied at the UoL Farm to determine
287 the mass flux of DOC and nitrate that represent the principal groundwater quality
288 indicators and contaminants in a KCZ (Goldscheider and Drew 2014; Figs. 2, 4). The
289 transect was applied avoiding faults where the bedrock can be assumed homogeneous
290 (Fig. 2a). The described approach represents the first application, as far as we are aware,
291 of the Transect Method to a Farm that we refer to as TMF. Given the concentration of the
292 chemical species in groundwater, C_i, the advective groundwater mass flux, M_{gw}, is
293 calculated as:

294

295 (1) $M_{gw} = C_{gw} \times Q_{gw}$

296

297 where Q is the groundwater flux defined by the Darcy's law as the product of the hydraulic
298 conductivity (K) and the hydraulic gradient (i) and transect area (A_2). Note that in the case
299 of the transect area defined in Figure 2, the hydraulic gradient (annual arithmetic average,
300 0.0236) is known from the monitoring of the three boreholes at the UoL Farm and the
301 aquifer hydraulic conductivity (arithmetic mean, 1.1 m/day; Fig. 3) from slug tests (Medici
302 et al. 2019a). Slug test values representative of the horizontal hydraulic conductivity show
303 arithmetic mean>geometric mean>median>harmonic mean. The arithmetic mean was
304 selected for use in this study, representing the highest mean, because the most highly
305 conductive layers dominate horizontal flow at the field site (Medici et al. 2019a).

306

Given the contaminant concentration (C_{sw}) of the specific chemical specie in soil water collected at the base of the soil profile at 0.35-0.45 m depth[1], the contaminant mass flux from the land surface through area A_1 (Fig. 4) is then defined as:

(2) $M_{inf} = C_{sw} \times Q_{inf}$

where Q_{inf} is the product of the recharge rate (i.e. precipitation minus evapotranspiration) and the area A_1. The annual average recharge rate used to calculate the hydrological flux from the land surface (Q_{inf}) is 0.134 m/year derived from the calibrated MODFLOW-2005 regional groundwater model previously used at the field site (Medici et al. 2019b). The use of unique recharge value is supported by the selection of a transect area that is overlain by uniform ~0.5 m thick well drained calcareous soil above a relatively homogenous bedrock, avoiding fault zones (Fig. 2a).

A theoretical 3D block (see Figures 1d, 2 and 4) has been created with the longer side oriented parallel to the annual groundwater Fisher mean vector (azimuth 68°; Medici et al. 2019a). The area used to compute the upstream groundwater flux (Q_{gw}) is defined by the parallelepiped side, L1 (Figure 2) and the aquifer saturated thickness of 30 m estimated by the British Geological Survey core logs (Cooper and Lawley, 2007, Fig. 4).

Our analysis assumes that the total mass flux (M_{mix}) of the two species leaving the transect area within groundwater is given by the sum of the groundwater flux entering the transect area (M_{gw}) and that infiltrating through the soil zone (M_{inf}) (Fig. 4). Median values of DOC and nitrate concentration (C_i) were calculated from the dataset available in the area of the transect to apply equations (1) and (2). Concentrations in groundwater from the Headley Hall Farm and BH2 borehole and the soil water concentrations collected at 0.40 mBGL (Figs. 2b, 4) were used to define C_{gw} and C_{sw} respectively. Note that, DOC and

[1] Samples were collected at the base of the soil zone to obtain concentrations of nitrate and DOC below the zone of potential denitrification and differential bacterial activity within the soil.

nitrate concentrations from Hadley Hall Farm and BH2 were selected due the upstream position of these boreholes with respect to the other boreholes of the UoL Farm, BH1 and BH3 (Fig. 2b). The Headley Farm is the shallowest borehole that the Environment Agency sample in the study area and is screened at the same depth interval of BH1, BH2 and BH3. The Headley Farm, BH1, BH2 and BH3 boreholes are all characterized by a 0.20 m diameter.

To test the validity of the TMF, the modelled DOC and nitrate mass fluxes were converted into concentrations dividing by the surface plus groundwater flux, Q_{mix} (Q_{gw}+Q_{in}). This conversion allows comparison with the measured concentration values acquired from the UoL Farm boreholes.

4.0 Results

4.1 Aquifer physiochemical properties

The mean, range and standard deviation for electrical conductivity, fluid temperature and pH for the different source waters are shown in Table 1. The mean pH of all the surface and groundwater samples was 7.4° and ranged from 6.5° to 8.0° (Fig. 1d). Mean fluid temperature collected from all the different sources of water was 10.0° and ranged from 9.2° up to 19.9°C (Fig. 1d). Electrical conductivity of the water samples displayed a wide range; from 140 up to 1558 µS/cm (n=276).

Comparison between the different sources of water indicates similarity in the pH and conductivity values between the shallow (0-40 mBGL) boreholes of the UoL and the soil waters from the arable and pasture fields as well as the springs. Overlap of electrical conductivity, fluid temperature and pH ranges indicates a good degree of hydraulic connectivity between the soil, shallow saturated aquifer zone and springs (Tab. 1). In contrast, pH, fluid temperature and electrical conductivity are higher in the groundwater sampled at depth from the EA boreholes, indicating a lower degree of hydraulic

358 connectivity with all sources of surface water. Fluid temperature and electrical conductivity
359 from the stream samples were more scattered compared to the other water sources,
360 probably due to contribution of external surface water sources and atmospheric control on
361 surface water temperature (Tab. 1).
362 The groundwater of the Cadeby Formation, shows a Ca^{2+}-Mg^{2+} bicarbonate-type
363 composition (Fig. 5). The order of abundance is $Ca^{2+}>Mg^{2+}>Na^{+}>Al^{3+}>Mn^{2+}>Fe^{2+}$ and
364 $HCO^{3-}>SO4^{2-}>Cl^{-}>NO_3^{-}$ for cations and anions, respectively. Binary diagrams, which
365 provide information on the chemical processes occurring in the Cadeby Formation, are
366 illustrated in Figure 6a-c. The Mg^{2+}-Ca^{2+} binary diagram shows positive correlation, which
367 lies above the 1:1 ratio (Fig. 6a). This trend is due to the higher abundance of more highly
368 soluble calcite with respect to dolomite (60% $CaCO_3$, 40% Mg_2CO_3) in the Cadeby
369 Formation of Yorkshire (Lott and Cooper, 2008). Na^{+}-Cl^{-} regression lines (Fig. 6b) are
370 parallel to the 1:1 ratio which indicates dissolution of halite, which is most likely related to
371 dissolution of evaporites within the Edlington Formation. The latter evaporitic formation is
372 juxtaposed against the Cadeby Formation by normal faults that behave as hydraulic
373 connectors (see Figs. 1c, 2).
374 Similarly, SO_4^{2-}-Ca^{2+} linear regression (Fig. 6c) indicates gypsum dissolution from the
375 evaporitic strata of the Edlington Formation (Moussa et al. 2014; Re et al. 2017). Note that,
376 the SO_4^{2-}-Ca^{2+} regression lines do not superimpose exactly on the 1:1 line for gypsum
377 dissolution due to additional Ca^{2+} input from dissolution of calcite in the Magnesian
378 Limestone Group. Springs show a higher concentration of Ca^{2+} with respect to
379 groundwater and streams (Fig. 6a, c).
380 The World Health Organization (WHO) drinking water quality limit for nitrate (50 mg/L) is
381 breached in many of the EA boreholes, springs and streams, and in the pasture soil water
382 samples (Fig. 7). The nitrate 75th percentile is also above the WHO limit in all the UoL
383 boreholes (Fig. 8).

Overall, nitrate concentration shows medians which are respectively above and below the WHO limit in the groundwater sampled from the UoL shallow (15-40 mBGL) boreholes versus those sampled from the deeper (20-112 mBGL) EA boreholes. Note, no consistent variation in nitrate concentrations with depth was recognized from the multiple depth intervals (8-40 mBGL) in the UoL boreholes. Nitrate concentrations however substantially decrease at greater depths >40 mBGL seen in samples from the EA boreholes (Fig. 7). Nitrate concentrations in the springs are very similar to that of the shallow UoL boreholes, whereas, nitrate concentrations in streams are lower than those in both the UoL boreholes and springs (and the upper percentile lies below the WHO limit, Fig. 7).

Nitrate concentrations in the soil water from the pasture fields are similar to those in the groundwater from the UoL boreholes (Fig. 7). This similarity suggests that leaching from these pasture soils which are upstream of the farm boreholes (see Fig 2) are a major nitrate source for groundwater of the studied Permian dolostone. Indeed, nitrate concentration is higher in pasture soil where livestock is present compared with arable land exclusively used to grow crops as shown in Figure 7. Nitrate concentrations are lower in streams compared with soil water and groundwater as illustrated in the box plot in Figure 7. This concentration difference may arise from dilution of the groundwater baseflow component of streamflow by freshwater runoff that is generated in correspondence of the low permeability units of the Pennine Coal Measure Group in the western sector of the study site (Fig. 1; Aldrick 1978).

Ranges, interquartile ranges and median concentration (C) of DOC are shown in Figure 9. Similar and highest DOC concentrations were observed in the soil water from the pasture (C_{median} = 13.0 mg/L) and arable (C_{median} = 11.0 mg/L) fields. Concentrations of DOC in the saturated zone of the aquifer were considerably smaller, with median values of 5.5 mg/L in groundwater from the UoL boreholes (15 to 35 mBGL) and 0.5 mg/L from the deeper (> 40 mBGL) EA boreholes. Here, the observed pattern of DOC in soil water, shallow and

deeper groundwater is consistent with infiltration from both the farm arable and pasture soils providing increased DOC to shallow (15 to 40 mBGL) groundwater. DOC concentrations observed at the shallower depth (8 - 40 mBGL) intervals sampled via the UoL Farm boreholes do not show evident depth variations. However, DOC varies seasonally from 1.0 up to 13.8 mg/L (Fig. 6) and shows a wider seasonal variation than the other solute chemical species, with higher concentrations observed in the spring-summer period from late April to June.

4.2 DOC and Nitrate mass fluxes

Mass fluxes of nitrate and DOC were modelled applying the TMF to a theoretical 3D block in the area of the UoL Farm (Figs. 2, 4). The inputs and outputs for this method are illustrated in Table 2 for 'background or inflowing' groundwater (Q_{gw}, M_{gw}), infiltrating recharge water (Q_{inf}, M_{inf}), and exiting groundwater (Q_{mix}, M_{mix}), in terms of DOC and nitrate fluxes. The initial step for this computation is the definition of the fluxes of recharge and groundwater flow (see Figure 4). The recharge flux (Q_{inf}) is the product of the annual average recharge rate from the calibrated MODFLOW-2005 model (see Figure 1c) and land surface area (A_1) applied at the top of the 3D block that represents a portion of the land surface (see Figure 4). The groundwater flux (Q_{gw}) is calculated from the annual average hydraulic gradient (0.0236) and arithmetic mean hydraulic conductivity (1.1 m/day) from slug tests applied to the saturated thickness of aquifer unit (Medici et al. 2019a). The sum of these two contributions (Q_{inf}, Q_{gw}) provides the outflowing groundwater flux (Q_{mix}) of 2292 m^3/day for the selected transect (Fig. 2b; Tab. 2).

Mass fluxes of nitrate and DOC were modelled from Q_{in}, Q_{out} by applying equations (1) and (2) (Tab. 2). Median concentrations of nitrate (Figs. 7, 8) and DOC (Fig. 9) from land surface and inflowing groundwater flow are assumed to be those from soil water (median

435 of all arable and pasture measurements) and from the EA Headley Hall Farm and BH2
436 boreholes that are located upstream with respect to the other two UoL boreholes (Fig. 2b).
437 The infiltrating mass fluxes (M_{inf}) are 4526 and 10454 kg yr^{-1} for DOC and nitrate,
438 respectively according to the proposed model. The transect is 200 hectares and therefore
439 infiltration mass fluxes can be expressed as 23 and 52 kg yr^{-1} ha^{-1} for DOC and nitrate,
440 respectively to enable comparison at the UoL as well as other farm areas across the world.
441 Applied nitrogen inputs from arable and pasture field are 190 and 180 kg yr^{-1} ha^{-1},
442 respectively. 52 kg yr^{-1} ha^{-1} of NO_3^- corresponds to 12 kg yr^{-1} ha^{-1} of N flux. This N value of
443 flux is derived from natural recharge and reaches the water table. Hence, ~6% of applied
444 nitrogen infiltrates in the saturated part of the aquifer.
445 The outflowing nitrate flux derived from equations (1) and (2) is 45202 kg yr^{-1} and contains
446 the inflowing mass flux, M_{gw} (34748 kg yr^{-1}; Tab. 2) as well as that infiltrating from the
447 transect. DOC outflowing mass flux is 5146 kg yr^{-1} as shown in Table 2. Notably, model
448 outputs show that $M_{inf}<M_{gw}$ for nitrate. This hydrochemical scenario contrasts the modelled
449 DOC mass fluxes that indicate $M_{inf} >>> M_{gw}$ (Tab. 2). The UoL Farm appears therefore to
450 be an evident point source of DOC and a more mild nitrate-polluter.
451 To test the validity of the TMF, the modelled DOC and nitrate mass fluxes are converted
452 into modelled downstream concentrations by dividing the groundwater flux leaving the site
453 downstream boundary, Q_{mix} (2292 m^3/day). The modelled concentrations for DOC and
454 nitrate are shown as dashed lines in Figures 7 and 8 (for nitrate) and 9 (for DOC). While
455 concentrations at the downstream boundary were not measured directly, these modelled
456 concentrations can be compared to the measured concentration in groundwater at the
457 BH1 and BH3 receptors (see Fig. 2b).
458 The modelled nitrate (54.0 mg/L) concentration from the transect calculation falls within the
459 interquartile range (53.0-71.5 mg/L) of nitrate for BH1 (Fig. 8). However, BH3 nitrate
460 concentrations lies above the model output of 54.0 mg/L, possibly due to the proximity of a

461 silage field that has received pig slurry (Figs. 2b, 8). The model also highlights that if the
462 median soil water nitrate concentration was reduced by 40% from 40.0 mg/L to 24.0 mg/L
463 the modelled out-flowing nitrate concentration in groundwater would fall below the 50 mg/L
464 that represents the limit imposed by the World Health Organization. Thus agricultural
465 practices in the arable and pasture fields need to be modified to reduce soil water nitrate
466 concentrations by this amount.
467 The modelled DOC (6.2 mg/L) concentration from transect calculation fall within the
468 interquartile ranges of DOC (3.0-10.3 and 2.2-11.7 mg/L for BH1 and BH3, respectively) in
469 the two receptors of the UoL (Fig. 9). Notably, the model outputs closely match the
470 arithmetic average of BH1 and BH3 boreholes for DOC. These results support validity of
471 the presented TMF approach (Figs. 7-9; Tab. 2).
472

473 **5. Discussion**

474 The influence of soil-derived nitrate and DOC on groundwater quality was studied in a
475 dolomitic KCZ at UoL Experimental Farm. From a hydrochemical point of view, analyses
476 reveal a baseline Ca^{2+}-Mg^{2+} bicarbonate-type water that represents the typical composition
477 of dolostone aquifers (Seyhan et al. 1985; Barbieri et al. 2005; Xanke et al. 2015).
478 Similarly, the range of nitrate (Fig. 7) and DOC (Fig. 9) concentrations from soil and
479 groundwater indicate a high degree of hydraulic connectivity between these two elements,
480 as commonly reported for a KCZ (Jourde et al. 2018); this is discussed further in section
481 5.1.
482 Hydraulic conductivity values of the Cadeby Formation increase from the core-log to the
483 scale of the field site. Groundwater flow models find calibration with values that overlap
484 those of pumping tests (Fig. 3; Schulze-Makuch et al. 1999; Gleeson et al. 2011). This
485 physical feature is typical for moderately karstified aquifers. As a consequence of the
486 common physiochemical features of the studied aquifer, this research shows how physical

hydrogeological parameters from modelling groundwater flow can be combined with hydrochemical analyses to develop approaches for modelling contaminant fluxes via KCZs under farmland.

5.1 Aquifer vulnerability

Nitrate and DOC are good indicators of aquifer vulnerability to contamination in areas dedicated to intense agriculture (Ducci 2010; Wachniew et al. 2016). DOC is an important parameter from the viewpoint of water quality at farm sites in karst areas (Moral et al. 2008; Goldscheider and Drew 2014; Koit et al. 2020). One reason for its importance is that DOC forms complexes with hydrophobic organic contaminants released by pesticides facilitating their transport (Wang et al. 2004, 2018).

In this paper, we have used DOC and nitrate concentrations in surface, soil and groundwater to characterize the flux of NO_3^- and DOC through the Permian dolostone of the Cadeby Formation (see conceptual model illustrated in Figure 10) and in doing so identified the most vulnerable depth interval of the aquifer. Pasture soil waters have much higher concentrations of nitrate than arable soil waters (the latter show values below the WHO drinking water limit). Nitrate concentrations decrease with depth from the pasture soil water to the shallow (<~40 mBGL) groundwater, and at depths > 40 mBGL nitrate concentrations are even lower; mostly below the WHO drinking water limit (Fig. 7). DOC concentrations are similar in arable and pasture soil waters, with lower concentrations in shallow (0-40 mBGL) groundwater (Figs. 9, 10). Note that, DOC also decreases at depths > 40 mBGL in the deep aquifer. Other studies have also reported a sharp decrease in both nitrate and DOC concentrations with depth in the KCZ in agricultural areas (Foster et al. 1982; Geyer et al. 1992).

Our research suggests that the zone of maximum aquifer vulnerability is in the first 40 m below the soil surface. This zone partially includes the most conductive (K=0.83-2.89

513 m/day) part of the aquifer that is in the depth interval 0-25 mBGL as indicated by multi-
514 level slug tests (Medici et al. 2019a). However, karstification is much more pervasive in
515 correspondence of normal fault zones intercepted in the area of the relatively deep
516 abstraction wells (Fig. 1c). These faults are more conductive in borehole tests (K_{median}= 35
517 m/day; n=7; Allen et al. 1997) and characterized by much faster modelled groundwater
518 velocities (3000-5500 m/day; Medici et al. 2019b) as typical in faulted dolostone aquifer
519 portions (Bauer et al. 2016). Intense karstification persists up to 40 m depth in
520 correspondence of these tectonized zones justifying a relatively deep vulnerable zone (see
521 Fig. 10).
522
523 *5.2 TMF and solute contaminant transport*
524 Mass fluxes of nitrate and DOC arising from agricultural practices at the farm, including pig
525 slurry spreading, were modelled using the TMF applying the rainfall recharge from the
526 calibrated regional MODFLOW-2005 flow model (Fig. 3; Medici et al. 2019b). Modelled
527 mean concentrations of DOC and nitrate in groundwaters down-gradient of the site are
528 within the range of those measured (Figs. 7-9; Tab. 2). The modelled nitrogen mass flux
529 (12 kg ha^{-1} yr^{-1}) driven by rainfall recharge indicates that ~6% of applied nitrogen (from pig
530 slurry plus mineral fertilisers) reaches the saturated part of the aquifer; a value that is in
531 the expected range of infiltration fractions (5%-50%) (Liao et al. 2012; Green et al. 2018).
532 Literature also supports the modelled values of nitrate flux in farmland. Indeed, nitrogen
533 fluxes applied to crops is ~10^1 kg ha^{-1} yr^{-1} in areas of the world dedicated to intense
534 agriculture (Messer and Brenzonic 1983; Jordan et al. 1998; Green et al. 2018). The TMF
535 therefore provides a reliable tool to compute solute mass fluxes leaving a farm site via the
536 groundwater pathway. Note that at this field site denitrification below the soil zone is
537 unlikely to be significant, which means that the assumption of the TMF that nitrate is
538 conserved within the aquifer is valid. This scenario is related to low groundwater

539 temperature (9° - 10°) that typically inhibits denitrification (Rivett al. 2008). Furthermore,
540 measured groundwater flow velocities which are very high (50 - 250 m/day, Medici et al.
541 2019a) and hence residence times in the aquifer are too low to allow significant
542 denitrification, as proposed by other authors for similar aquifers across the world (Moon et
543 al. 2006; Goldscheider and Drew, 2014; Hartmann et al. 2014; Yang et al. 2020).
544 Nitrate and DOC concentrations in soil and groundwater are known to vary temporally and
545 spatially due to variations in hydrology, soil physical and chemical properties, crop rotation
546 and fertilizer inputs (Sieling et al. 1997, Lord et al. 1999; Williams et al. 2000). In recent
547 years, there has been concerted efforts to improve the nitrogen use efficiency of both
548 inorganic fertilisers and manure/slurry applications in order to help reduce nitrate leaching.
549 In 2000, Chambers et al. (2000) reported that about 50% of pig and poultry manures are
550 applied in the autumn (August-October) to cereal stubble in the UK. However, they also
551 found that highest nitrate losses occurred following the application of slurry to winter
552 cereals in the autumn. This practice is applied at the UoL Farm and here more nitrate is
553 available for leaching. Pig slurry application is going to change at the studied farm in the
554 near future. In fact, in recent years, advice to UK farmers has focussed on getting them to
555 switch from autumn to spring applications for high readily-available-N manures and slurry
556 (Chambers et al. 2000; Ball Coelho et al. 2006).
557 This research develops the application of the Transect Method, previously used for
558 prediction of impacts of industrial sources on groundwater quality, to other point sources of
559 contamination such as farms. Previous applications of the Transect Method focused on
560 prediction of contaminant mass fluxes and concentration at industrial field sites related to
561 release of chlorinated pollutants and heavy metals (Verreydt et al. 2012, 2013; Padgett et
562 al. 2017). Here we show that the Transect Method can be used to define mass fluxes and
563 hence concentrations of contaminants in groundwater. The approach provides an
564 indication of whether a particular point source (in this case a farm where pig slurry

565 spreading occurs) has a significant impact on the contamination load in groundwater. In
566 our case, the results show that the farm has a significant impact on groundwater DOC
567 concentrations, and to a lesser extent nitrate concentrations (see Tab. 2). This scenario is
568 related to surrounding farms use of inorganic fertilisers so regional groundwater nitrate
569 concentrations are already relatively high, whereas pig slurry spreading is less common in
570 the immediate vicinity of the UoL Farm. In fact, pig slurry is practiced at this farm because
571 the indoor pig unit at the farm provides a ready supply.
572 The TMF could also be used to define the boundary conditions for solute transport models
573 (e.g., Goltz et al. 2007) for prediction of downstream impacts for example at well
574 abstractions at the study site. Thus, the future modelling of reactive contaminant transport
575 at the UoL Farm must primarily focus on the first and highly vulnerable ~40 meters below
576 the ground using different concentrations of nitrate and DOC in soil and groundwater (Fig.
577 10).
578

579 **6.0 Conclusions**

580 Nitrate and DOC are considered two key chemical species that determine water quality in
581 the CZ in karstic environments. Here, we propose an approach to demonstrate how the
582 combination of hydrochemical analyses of different water sources from multiple depths,
583 combined with physical groundwater flow model characterisation allows prediction of mass
584 fluxes of DOC and nitrate from farmland via the groundwater pathway. A robust hydraulic
585 characterisation reveals the mechanisms of solute transport and facilitates future
586 modelling scenarios. In this paper, the KCZ of the Permian dolostone of NE Yorkshire (NE
587 England, UK) has been used and the Transect Method applied to compute nitrate and
588 DOC mass fluxes at the study site (the University of Leeds Farm, Yorkshire, UK). This
589 methodology is used to predict the impacts of farm activity on concentrations of pollutant
590 species in groundwater. The transect approach is here applied for the first time to a farm-

591 source of contaminations where pig slurry is applied in the autumn when leaching losses
592 are highest to both cereal crops, and pasture fields (post cutting for silage). The use of this
593 methodology was validated by comparing the modelled concentrations of DOC and nitrate
594 with measured concentrations in groundwater. The results show that the farm activity
595 influences the 'background' concentrations of both DOC and nitrate in groundwater. The
596 influence on DOC is most marked, because this farm uses pig slurry rather than only
597 inorganic fertilisers, which is more common for the surrounding farms.
598 The hydrochemical analysis of groundwater highlights that the zone of highest vulnerability
599 to contamination to the first ~40 meters below the ground surface is due to higher
600 concentrations of nitrate and DOC being observed in this zone. This zone also had high
601 hydraulic conductivity of karst fissures and conduits in the first ~15 meters below the water
602 table that most likely vertically extends to greater depths in faulted areas. Hence, future
603 modelling of KCZ contaminant transport should primarily focus in the first ~40 meters
604 below the ground.
605 Following this research, we envisage to export the TMF that combines a groundwater
606 model-derived recharge, baseline soil water and groundwater analyses and computation of
607 mass fluxes to support conceptualization and modelling of contaminant transport in other
608 karst areas.
609

610 **Acknowledgements**

611 The work represents a synthesis of 15 years of hydrochemical and hydrological research
612 at the UoL Farm. Funding is acknowledged from the Natural Environment Research
613 Council via the CZO: Using Critical Zone Science-Peri-Urban Agriculture in China and the
614 Soil Security Programme grants, and the Faculty of Environment via funding to support
615 MSc Student Dissertation research. Hence, the support of MSc students Zeyu Ao and
616 Christian Walker that have collected some of the field data was especially appreciated.

617 Edward Wrathmell (Environment Agency of England) gave assistance with hydrochemical
618 licensing issues and provision of data under licence. We also thank Rachael Spraggs
619 (University of Leeds) for arranging data access licensing. We are grateful to managers
620 and operators at the UoL Farm for supporting our work, particularly George Sorensen for
621 planning borehole instrumentation, Richard Grayson, Sarah Hunt and Martin Lappage for
622 collecting the soil water samples and David Ashley for analysing them. However, Rachel
623 Gasior analysed the groundwater samples from the UoL boreholes. This research also
624 benefited from discussions with Kent Keller (Washington State University) and Beth
625 Parker (University of Guelph), regarding transport of toxic compounds in the Karst Critical
626 Zone. Finally, guidance from Editor-in-Chief Corrado Corradini and comments from three
627 anonymous reviewer have substantially improved the manuscript.

628

629 **References**

630 Aldrick, R.J., 1978. The hydrogeology of the Magnesian Limestones in Yorkshire between
631 the River Wharfe and the River Aire. Quart. J. Engineer. Geol. Hydrogeol. 11(2), 193-201.

632 Allen-King, R.M., Grathwohl, P., Ball, W.P., 2002. New modeling paradigms for the
633 sorption of hydrophobic organic chemicals to heterogeneous carbonaceous matter in soils,
634 sediments, and rocks. Advan. Water Resour. 25(8-12), 985-1016.

635 Anderson, S.P., Hinckley, E.L., Kelly, P., Langston, A., 2014. Variation in critical zone
636 processes and architecture across slope aspects. Procedia Earth Planet. Sci. 10, 28-33.

637 Allen, D.J., Brewerton, L.M., Coleby, B.R., Gibbs, M.A., Lewis, A., MacDonald, S.J.,
638 Wagstaff, A.T., Williams, L.J., 1997. The Physical Properties of Major Aquifers in England
639 and Wales. Technical Report WD/97/34, 157-287. British Geological Survey, Nottingham,
640 England (UK).

641 Ball Coelho, B.R., Roy, R.C., Bruin, A.J., 2006. Nitrogen recovery and partitioning with
642 different rates and methods of sidedressed manure. Soil Sci. Soc. Am. J. 70(2), 464-473.

643 Banwart, S., Bernasconi, S.M., Bloem, J., Blum, W., Brandao, M., Brantley, S., Chabaux,
644 F., Duffy, C., Kram, P., Lair, G., Lundin, L., 2011. Soil Processes and Functions in Critical
645 Zone Observatories: Hypotheses and Experimental. Vadose Zone J. 10(3):974-987.

646 Banwart, S.A., Bernasconi, S.M., Blum, W.E., de Souza, D.M., Chabaux, F., Duffy, C.,
647 Kercheva, M., Krám, P., Lair, G.J., Lundin, L., Menon, M., 2017. Soil functions in Earth's
648 critical zone: key results and conclusions. Adv. Agron. 142, 1-27.

649 Barbieri, M., Boschetti, T., Petitta, M., Tallini, M., 2005. Stable isotope (2H, 18O and
650 87Sr/86Sr) and hydrochemistry monitoring for groundwater hydrodynamics analysis in a
651 karst aquifer (Gran Sasso, Central Italy). Appl. Geochem. 20(11), 2063-2081.

652 Bauer, H., Schröckenfuchs, T.C. Decker, K., 2016. Hydrogeological properties of fault
653 zones in a karstified carbonate aquifer (Northern Calcareous Alps, Austria). Hydrogeol.
654 J. 24(5), 1147-1170.

655 Bicalho, C.C., Batiot-Guilhe, C., Seidel, J.L., Van Exter, S., Jourde, H., 2012 Geochemical
656 evidence of water source characterization and hydrodynamic responses in a karst aquifer.
657 J. Hydrol. 450, 206-218

658 Borović, S., Terzić, J., Pola, M., 2019. Groundwater quality on the adriatic karst Island of
659 Mljet (croatia) and its implications on water supply. Geofluids 2019.
660 https://doi.org/10.1155/2019/5142712

661 Brantley S.L., Eissenstat D.M., Marshall J.A., Godsey S.E., Balogh-Brunstad Z., Karwan
662 D.L., Papuga S.A., Roering J., Dawson T.E., Evaristo J., Chadwick O., 2017. Reviews and
663 syntheses: on the roles trees play in building and plumbing the critical zone. Biogeosci. 17,
664 14(22).

665 Chambers, B.J., Smith, K.A., Pain, B.F., 2000. Strategies to encourage better use of
666 nitrogen in animal manures. Soil Use Manage. 16, 157-166.

667 Cooper, A.H., Lawley, R.S., 2007. Tadcaster Magnesian Limestone 3-D borehole
668 interpretation and cross-sections study. British Geological Survey, Nottingham, England
669 (UK).

670 Defra, 2002. The Government's strategic review of diffuse water pollution from agriculture
671 in England and Wales. Department for Environment, Food and Rural Affairs, London

672 Dong, X., Cohen, M.J., Martin, J.B., McLaughlin, D.L., Murray, A.B., Ward, N.D., Flint,
673 M.K., Heffernan, J.B., 2018. Ecohydrologic processes and soil thickness feedbacks control
674 limestone-weathering rates in a karst landscape. Chemical Geol., 118774.

675 Ducci, D., 2010. Aquifer Vulnerability assessment methods: the non-independence of
676 parameters problem. J. Water Resour. Protect. 2(4)

677 Emblanch, C., Zuppi, G.M., Mudry, J., Blavoux, B., Batiot, C., 2003. Carbon 13 of TDIC to
678 quantify the role of the unsaturated zone: the example of the Vaucluse karst systems
679 (Southeastern France). J Hydrol. 279(1-4), 262-274.

680 Falcone, R.A., Falgiani, A., Parisse, B., Petitta, M., Spizzico, M., Tallini, M., 2008.
681 Chemical and isotopic (δ18O‰, δ2H‰, δ13C‰, 222Rn) multi-tracing for groundwater
682 conceptual model of carbonate aquifer (Gran Sasso INFN underground laboratory–central
683 Italy). J. Hydrol. 357(3-4), 368-388.

684 Fezzi, C., Hutchins, M.G., Rigby, D., Bateman, I.J., Posen, P., Hadley, D., 2010.
685 Integrated assessment of water framework directive nitrate reduction measures. Agric.
686 Econ. 41(2), 123-134

687 Ford, D.C., Williams, P.W., 1989. Karst geomorphology and hydrology, Unwin Hyman,
688 London (UK).

689 Foster, S.S.D., 1976. The vulnerability of British groundwater resources to pollution by
690 agriculture leachates. MAFF Tech. Bull. 32, 159-165.

691 Forster, S.S.D., Cripps, A.C., Smith-Carington, A., 1982. Nitrate leaching to
692 groundwater. Philosoph. Transact. Royal Soc. 296, 477-489.

693 Geyer, D.J., Keller, C.K., Smith, J.L., Johnstone, D.L., 1992. Subsurface fate of nitrate as
694 a function of depth and landscape position in Missouri Flat Creek watershed, USA. J.
695 Contam. Hydrol. 11(1-2), 127-147.

696 Goldscheider, N., Drew, D., 2014. Methods in Karst hydrogeology: IAH: international
697 contributions to hydrogeology, 26. Crc Press.

698 Goltz, M.N., Kim, S., Yoon, H., Park, J., 2007. Review of groundwater contaminant mass
699 flux measurement. Environ. Engineer. Res. 12(4), 176-193.

700 Goss, M.J., Barry, D.A.J., Rudolph, D.L., 1998. Contamination in Ontario farmstead
701 domestic wells and its association with agriculture: 1. Results from drinking water wells. J.
702 Contam. Hydrol. 32(3-4), 26-293.

703 Gleeson, T., Smith, L., Moosdorf, N., Hartmann, J., Dürr, H.H., Manning, A.H., van Beek,
704 L.P., Jellinek, A.M., 2011. Mapping permeability over the surface of the Earth. Geophys.
705 Res. Let. 38(2).

706 Green, S.M., Dungait, J.A., Tu, C., Buss, H.L., Sanderson, N., Hawkes, S.J., Xing, K., Yue,
707 F., Hussey, V.L., Peng, J., Johnes, P., 2019. Soil functions and ecosystem services
708 research in the Chinese karst Critical Zone. Chem. Geol. 527, 119107.

709 Green, C.T., Liao, L., Nolan, B.T., Juckem, P.F., Shope, C.L., Tesoriero, A.J., Jurgens,
710 B.C., 2018. Regional variability of nitrate fluxes in the unsaturated zone and groundwater,
711 Wisconsin, USA. Water Resour Res. 54(1), 301-322.

712 Hartmann, A., Goldscheider, N., Wagener, T., Lange, J., Weiler, M., 2014. Karst water
713 resources in a changing world: Review of hydrological modeling approaches. Rev.
714 Geophys. 52(3), 218-242.

715 Hill, M.E., Stewart M.T., Martin, A., 2010 Evaluation of the MODFLOW-2005 conduit flow
716 process. Groundwater 48(4), 549-559.

717 Holden, J., Grayson, R.P., Berdeni, D., Bird, S., Chapman, P.J., Edmondson, J.L., Firbank,
718 L.G., Helgason, T., Hodson, M.E., Hunt S.F.P., Jones, D.T., 2019. The role of hedgerows in
719 soil functioning within agricultural landscapes. Agricultur. Ecosyst. Environm. 273, 1-12.

720 Huang, W., Yu, H., Weber Jr, W.J., 1998. Hysteresis in the sorption and desorption of
721 hydrophobic organic contaminants by soils and sediments: 1. A comparative analysis of
722 experimental protocols. J. Contam. Hydrol. 31(1-2), 129-148.

723 Huebsch, M., Horan, B., Blum, P., Richards, K.G., Grant, J., Fenton, O., 2013. Impact of
724 agronomic practices of an intensive dairy farm on nitrogen concentrations in a karst aquifer
725 in Ireland. Agric. Ecosyst. Environ. 179, 187-199.

726 Hutchins, M.G., 2012, What impact might mitigation of diffuse nitrate pollution have on
727 river water quality in a rural catchment?. J. Environ. Manage. 109, 19-26

728 Jiang Z., Zhang C., Qin X, Pu J, Bai, B., 2019. Structural Features and Function of the
729 Karst Critical Zone. Acta Geol. Sin. 93, 109-112

730 Jordan, T.E., Weller, D.E., Correll, D.L., 1998. Denitrification in surface soils of a riparian
731 forest: Effects of water, nitrate and sucrose additions. Soil Biol. Biochem. 30(7), 833-843.

732 Jourde, H., Massei, N., Mazzilli, N., Binet, S., Batiot-Guilhe, C., Labat, D., Steinmann, M.,
733 Bailly-Comte, V., Seidel, J.L., Arfib, B., Charlier, J.B., 2018. SNO KARST: A French
734 network of observatories for the multidisciplinary study of critical zone processes in karst
735 watersheds and aquifers. Vadose Zone J. 17(1).

736 Keller, C.K., 2019. Carbon Exports from Terrestrial Ecosystems: A Critical-Zone
737 Framework. Ecosyst. 22(8), 1691-1705.

738 Koit, O., Barberá, J.A., Marandi, A., Terasmaa, J., Kiivit, I.K., Martma, T., 2020.
739 Spatiotemporal assessment of humic substance-rich stream and shallow karst aquifer
740 interactions in a boreal catchment of northern Estonia. J. Hydrol. 580,.12423

741 Kogovsek, J., Petric, M., 2014. Solute transport processes in a karst vadose zone
742 characterized by long-term tracer tests (the cave system of Postojnska Jama, Slovenia). J.
743 Hydrol. 519, 1205-1213

744 Kuntz, B.W., Rubin, S., Berkowitz, B. Singha, K., 2011. Quantifying solute transport at the
745 shale hills critical zone observatory. Vadose Zone J. 10(3), 843-857.

746 Lastennet, R., Mudry, J., 1997. Role of karstification and rainfall in the behavior of a
747 heterogeneous karst system. Environ. Geol. 32(2), 114-123.

748 Lerch, R.N., Groves, C.G., Polk, J.S., Miller, B.V., Shelley, J., 2018. Atrazine Transport
749 through a Soil–Epikarst System. J. Environ. Qual. 47(5), 1205-1213.

750 Lian, B., Yuan, D., Liu, Z., 2011. Effect of microbes on karstification in karst
751 ecosystems. Chinese Sci. Bullet., 56(35), 3743-3747.

752 Liao, L., Green, C.T., Bekins, B.A., Böhlke, J.K., 2012. Factors controlling nitrate fluxes in
753 groundwater in agricultural areas. Water Resour. Resear. 48(6).
754 https://doi.org/10.1029/2011WR011008

755 Lord, E.I., Johnson, P.A., Archer, J.R., 1999. Nitrate sensitive areas: a study of large scale
756 control of nitrate loss in England. *Soil Use and Management*, *15*(4), pp.201-207.

757 Lott G.K., Cooper, A.H., 2005 The building limestones of the Upper Permian, Cadeby
758 Formation (Magnesian Limestone) of Yorkshire. Report IR/05/048, British Geological
759 Survey, Nottingham (UK)

760 Mahler, B., Massei, N., 2007. Anthropogenic contaminants as tracers in an urbanizing
761 karst aquifer. J. Contam. Hydrol. 91(1-2), 81-106.

762 Mawson, M., Tucker, M., 2009. High-frequency cyclicity (Milankovitch and millennial-scale)
763 in slope-apron carbonates: Zechstein (Upper Permian), North-east
764 England. Sedimentology, 56(6), 1905-1936.

765 Medici, G., West, L.J., Mountney, N.P., 2016. Characterizing flow pathways in a sandstone
766 aquifer: tectonic vs sedimentary heterogeneities. Journal of Contaminant Hydrology, 194,
767 36-58.

768 Medici, G., West, L.J., Banwart, S.A., 2019a. Groundwater flow velocities in a fractured
769 carbonate aquifer-type: implications for contaminant transport. J. Contam. Hydrol. 222, 1-
770 16

771 Medici, G., West, L.J., Chapman, P.J., Banwart, S.A., 2019b. Prediction of contaminant
772 transport in fractured carbonate aquifer types: a case study of the Permian Magnesian
773 Limestone Group (NE England, UK). Environ. Sci. Pollution Res. 26(24), 24863-24884.

774 Mellander, P.E., Jordan, P., Wall, D.P., Melland, A.R., Meehan, R., Kelly, C., Shortle, G.,
775 2012. Delivery and impact bypass in a karst aquifer with high phosphorus source and
776 pathway potential. Water Resear. 46(7), 2225-2236.

777 Messer, J., Brezonik, P.L., 1983. Comparison of denitrification rate estimation techniques
778 in a large, shallow lake. Water Resear. 17(6), 631-640.

779 Moon, H.S., Nam, K., Kim, J.Y., 2006. Initial alkalinity requirement and effect of alkalinity
780 sources in sulfur-based autotrophic denitrification barrier system. J. Environ. Engineer.
781 132(9), 971-975.

782 Moral, F., Cruz-Sanjulián, J.J., Olías, M., 2008. Geochemical evolution of groundwater in
783 the carbonate aquifers of Sierra de Segura (Betic Cordillera, southern Spain). J.
784 Hydrol. 360(1-4):281-296.

785 Moussa, A.B., Mzali, H., Zouari, K., Hezzi, H., 2014. Hydrochemical and isotopic
786 assessment of groundwater quality in the Quaternary shallow aquifer, Tazoghrane region,
787 north-eastern Tunisia. Quatern. Int. 338, 51-58.

788 Murphy, P.J., 2000. The karstification of the Permian strata east of Leeds. Proceed. York.
789 Geol. Soc. 53(1), 25-30.

790 Murphy, P.J., Cordingley, J.N., 2010. Mass movement caves in northern England. Proc.
791 Univ. Bristol Spelaeol. Soc. 25(1):105-112.

792 Odling N.E., Gillespie, P., Bourgine, B., Castaing, C., Chiles, J.P., Christensen, N.P., Fillion
793 E., Genter, A., Olsen, C., Thrane, L., Trice, R., 1999. Variations in fracture system
794 geometry and their implications for fluid flow in fractured hydrocarbon reservoirs. Petrol.
795 Geosci. 5(4), 373-84.

796 Padgett, M.C., Tick, G.R., Carroll, K.C., Burke, W.R., 2017. Chemical structure influence
797 on NAPL mixture nonideality evolution, rate-limited dissolution, and contaminant mass
798 flux. J. Contam. Hydrol. 198, 11-23.

799 Panno, S.V., Hackley, K.C., Hwang, H.H., Kelly, W.R., 2001. Determination of the sources
800 of nitrate contamination in karst springs using isotopic and chemical indicators. Chem.
801 Geol. 179, 113-128.

802 Peyraube, N., Lastennet, R., Denis, A., 2012. Geochemical evolution of groundwater in the
803 unsaturated zone of a karstic massif, using the PCO2–SIc relationship. J. Hydrol. 430, 13-
804 24.

805 Peyraube, N., Lastennet, R., Denis, A., Malaurent, P., 2013. Estimation of epikarst air
806 PCO2 using measurements of water δ13CTDIC, cave air PCO2 and δ13CCO2. Geochim.
807 Cosmochim. Acta, 118, 1-17.

808 Piper A.M., 1953 A graphic procedure in the geochemical interpretation of water analysis.
809 Groundwater Note 12. United States Geological Survey. Reston, Virginia (USA).

810 Re, V., Sacchi, E., Kammoun, S., Tringali, C., Trabelsi, R., Zouari, Daniele, S., 2017.
811 Integrated socio-hydrogeological approach to tackle nitrate contamination in groundwater
812 resources. The case of Grombalia Basin (Tunisia). Sci. Total Environ. 593, 664-676.

813 Rivett, M.O., Buss, S.R., Morgan, P., Smith, J.W.N., Bemment, C.D., 2008. Nitrate
814 attenuation in groundwater: a review of biogeochemical controlling processes. Water Res.
815 42, 4215-4232.

816 Ryan, M., Meiman, J., 1996. An examination of short-term variations in water quality at a
817 karst spring in Kentucky. Groundwater, 34(1), 23-30.

818 Schulze-Makuch, D., Carlson, D.A., Cherkauer, D.S., Malik, P., 1999. Scale dependency
819 of hydraulic conductivity in heterogeneous media. Groundwater 37(6), 904-919.

820 Seyhan, E., Van De Griend, A.A., Engelen, G.B., 1985. Multivariate analysis and
821 interpretation of the hydrochemistry of a dolomitic reef aquifer, northern Italy. Water
822 Resour. Res. 21(7), 1010-1024.

823 Sieling, K., Günther-Borstel, O., Hanus, H., 1997. Effect of slurry application and mineral
824 nitrogen fertilization on N leaching in different crop combinations. J. Agric. Sci. 128(1), 79-
825 86.

826 Siemens, J., Haas, M., Kaupenjohann, M., 2003. Dissolved organic matter-induced
827 denitrification in subsoils and aquifers? Geoderma 113, 253-271.

828 Smith, D.B., Harwood, G.M., Pattison, J., Pettigrew, T.H., 1986 A revised nomenclature for
829 Upper Permian strata in eastern England. Geol. Soc. London Spec. Publ. 22, 9-17.

830 Sullivan, T.P., Gao, Y., Reimann, T., 2019. Nitrate transport in a karst aquifer: Numerical
831 model development and source evaluation. J Hydrol. 573, 432-448

832 Torresan, F., Fabbri, P., Piccinini, L., Dalla Libera, N., Pola, M., Zampieri, D., 2020.
833 Defining the hydrogeological behavior of karst springs through an integrated analysis: a
834 case study in the Berici Mountains area (Vicenza, NE Italy). Hydrogeol. J. 1-19

835 Tremosa, J., Debure, M., Narayanasamy, S., Redon, P.O., Jacques, D., Claret, F.,
836 Robinet, J.C., 2020. Shale weathering: a lysimeter and modelling study for flow, transport,
837 gas diffusion and reactivity assessment in the critical zone. J. Hydrol. 124925.

838 Tucker, M.E., 1991. Sequence stratigraphy of carbonate-evaporite basins: models and
839 application to the Upper Permian (Zechstein) of northeast England and adjoining North
840 Sea. J. Geol. Soc. 148(6), 1019-1036.

841 Xanke, J., Goeppert, N., Sawarieh, A., Liesch, T., Kinger, J., Ali, W., Hötzl, H., Hadidi, K.,
842 Goldscheider, N., 2015. Impact of managed aquifer recharge on the chemical and isotopic
843 composition of a karst aquifer, Wala reservoir, Jordan. Hydrogeol. J. 5, 1027–1040.

844 Verreydt, G., Annable, M.D., Kaskassian, S., Van Keer, I., Bronders, J., Diels, L.,
845 Vanderauwera, P., 2013. Field demonstration and evaluation of the Passive Flux Meter on
846 a CAH groundwater plume. Environ. Sci. Pollut. Resear. 20(7), 4621-4634.

847 Verreydt, G., Van Keer, I., Bronders, J., Diels, L., Vanderauwera, P., 2012. Flux-based risk
848 management strategy of groundwater pollutions: the CMF approach. Environ. Geochem.
849 Health 34(6), 725-736.

850 Wachniew, P., Zurek, A.J., Stumpp, C., Gemitzi, A., Gargini, A., Filippini, M., Rozanski, K.,
851 Meeks, J., Kværner, J., Witczak, S., 2016. Toward operational methods for the

852 assessment of intrinsic groundwater vulnerability: A review. Crit. Rev. Env. Sci.
853 Tec. 46(9):827-884.

854 Wakida, F.T., Lerner, D.N., 2005. Non-agricultural sources of groundwater nitrate: a review
855 and case study. Water Resear. 39(1), 3-16.

856 Wang, Z., Chen, M., Zhang, L., Wang, K., Yu, X., Zheng, Z., Zheng, R., 2018. Sorption
857 behaviors of phenanthrene on the microplastics identified in a mariculture farm in
858 Xiangshan Bay, southeastern China. Sci. Total Environ. 628, 1617-1626.

859 Wang, H., Magesan, G.N., Bolan, N.S., 2004. An overview of the environmental effects of
860 land application of farm effluents. New Zeal. J. Agr. Res., 47(4), 389-403.

861 Wang, L., Stuart, M.E., Lewis, M.A., Ward, R.S., Skirvin, D., Naden, P.S., Collins, A.L.,
862 Ascott, M.J., 2016. The changing trend in nitrate concentrations in major aquifers due to
863 historical nitrate loading from agricultural land across England and Wales from 1925 to
864 2150. Sci. Total Environ. 542, 694-705.

865 Ward, K., 2020. Slurry analysis results at the University of Leeds Farm and surrounding
866 areas. NRM Laboratories, Report 84722

867 Weber Jr, W.J., Huang, W., Yu, H., 1998. Hysteresis in the sorption and desorption of
868 hydrophobic organic contaminants by soils and sediments: 2. Effects of soil organic matter
869 heterogeneity. J. Contam. Hydrol. 31(1-2), 149-165.

870 Williams, T.M., Gresham, C.A., 2000. Nitrogen accumulation and changes in nitrate
871 leaching after 4 years of intensive forest culture on marginal agricultural land. NZ Forestry
872 Sci. 30, 266-279.

873 Worthington S.R., Smart C.C., Ruland, W., 2012. Effective porosity of a carbonate aquifer
874 with bacterial contamination: Walkerton, Ontario, Canada. J. Hydrol. 464, 517-527.

875 Yang, P., Wang, Y., Wu, X., Chang, L., Ham, B.,Song, L., Groves, C., 2020. Nitrate
876 Sources and biogeochemical processes in karst underground rivers impacted by different
877 anthropogenic input characteristics, Environ. Pollut. 265, 114835.

878 Zhang, Z., Chen, X., Soulsby, C., 2017. Catchment-scale conceptual modelling of water
879 and solute transport in the dual flow system of the karst critical zone. Hydrol.
880 Process. 31(19), 3421-3436.

881 Zhou, Q., Chen, L., Singh, V.P., Zhou, J., Chen, X., Xiong, L., 2019. Rainfall-runoff
882 simulation in karst dominated areas based on a coupled conceptual hydrological model. J.
883 Hydrol. 573, 524-533.

884

885 **Tables**

886 **Table 1** Fluid temperature, electrical conductivity and pH arithmetic mean, range and
887 standard deviation (σ) for the UoL and the EA boreholes, springs, streams and arable and
888 pasture fields

889 **Table 2** Input and output parameters for computation of mass fluxes of DOC and nitrate.

890

891 **Figures**

892 **Fig. 1** The study site of the UoL Farm in the area of Leeds and York and the dolostone
893 aquifer-unit of the Cadeby Formation. (a) The Permian Zechstein Basin and deposition of
894 the shallow water deposits of the Cadeby Formation (from Mawson and Tucker 2009); (b)
895 Great Britain with location of the study area (basemap from GeoMapApp); (c) Map of the
896 bedrock lithology with the location of the UoL Farm site, transect for computation of nitrate-
897 DOC mass fluxes and MODFLOW-2005 model of the study area (Medici et al. 2019b); (d)
898 Location of sampled streams, springs and boreholes.

899 **Fig. 2** Study site and detail of the transect. (a) Bedrock geology and studied boreholes, (b)
900 Sampling points used for computation of nitrate-DOC mass fluxes.
901 **Fig. 3** Hydraulic conductivity vs. scale for the Cadeby Formation at the study site.
902 **Fig. 4** Theoretical 3D block for calculation of nitrate and DOC mass fluxes at the study
903 site.
904 **Fig. 5** Piper diagram for water samples from boreholes, springs and streams.
905 **Fig. 6** Binary diagrams for springs, boreholes and streams; **a** Cl^--Na^+, **b** Mg^{2+}-Ca^{2+}, **c** SO^{4-}
906 - Ca^{2+}
907 **Fig. 7** Model output vs. concentrations of nitrates in samples from soil moisture, springs,
908 streams and boreholes
909 **Fig. 8** Model output vs. concentrations of nitrate in the EA Headley Farm wells, and BH1,
910 BH2 and BH3 boreholes of the UoL Farm.
911 **Fig. 9** Model output vs. concentrations of DOC in samples from soil moisture, springs and
912 boreholes
913 **Fig. 10** Hydrogeological conceptual scheme of the KCZ of at the UoL Farm site
914
915
916
917
918
919
920

Data source	pH	Fluid Temperature (℃)	Electrical Conducivity (µS/cm)
	Mean; Range; σ	Mean; Range; σ	Mean; Range; σ
University of Leeds boreholes	7.3; 7.0-7.6; 0.1	10.2; 9.2-11.4; 0.11	880; 775-1086; 95
EA Borehole	7.9; 7.4- 8.0; 0.2	18.1; 16.2-19.9; 3.4	890; 660-1170; 167
Spring	7.2; 7.0-7.7; 0.2	12.1; 9.8-19.3; 2.3	972; 640-1558; 281
Stream	7.4; 7.4-7.9; 0.2	13.9; 10.5-17.9; 1.5	817; 443-1154; 817
Arable Soil	7.6; 6.9-7.9; 0.3	N/A	670; 280-1070; 208
Pasture Soil	7.1; 6.5-8.0; 0.9	N/A	540; 140-790; 93

921 Table 1

922

Water Fluxes (Input)		Q_{inf} (m^3/day)	Q_{gw} (m^3/day)	Q_{mix} (m^3/day)
		734	1558	2292
Mass Fluxes (Output)	Chemical Specie	M_{in}	M_{gw}	M_{mix}
	Nitrate (kg yr^{-1})	16900	34748	51648
	DOC (kg yr^{-1})	4526	620	5146

923 Table 2

924

925

926

927

928

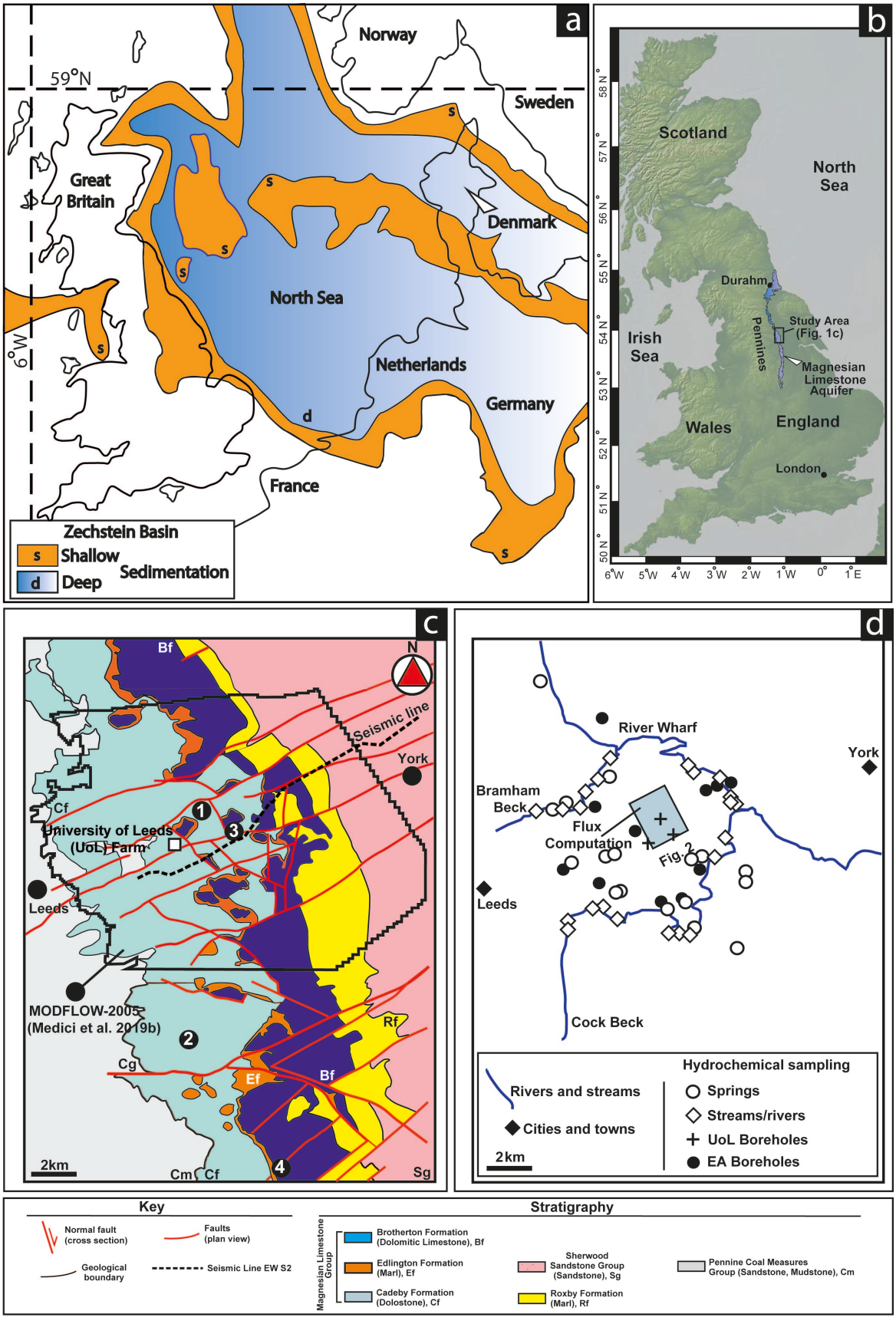
a
Norway
Sweden
59°N
Great Britain
Denmark
North Sea
Netherlands
Germany
France
6°W
Zechstein Basin
Shallow
Deep
Sedimentation
b
Scotland
North Sea
Irish Sea
Durahm
Study Area (Fig. 1c)
Pennines
Magnesian Limestone Aquifer
Wales
England
London
c
Bf
N
Seismic line
York
Cf
University of Leeds (UoL) Farm
Leeds
MODFLOW-2005 (Medici et al. 2019b)
Rf
Cg
Ef
Bf
2km
Cm
Cf
Sg
d
River Wharf
York
Bramham Beck
Flux Computation
Fig. 2
Leeds
Cock Beck
Hydrochemical sampling
Rivers and streams
Springs
Streams/rivers
Cities and towns
UoL Boreholes
EA Boreholes
2km
Key
Normal fault (cross section)
Faults (plan view)
Geological boundary
Seismic Line EW S2
Stratigraphy
Magnesian Limestone Group
Brotherton Formation (Dolomitic Limestone), Bf
Edlington Formation (Marl), Ef
Cadeby Formation (Dolostone), Cf
Sherwood Sandstone Group (Sandstone), Sg
Roxby Formation (Marl), Rf
Pennine Coal Measures Group (Sandstone, Mudstone), Cm

929

930 Fig. 1

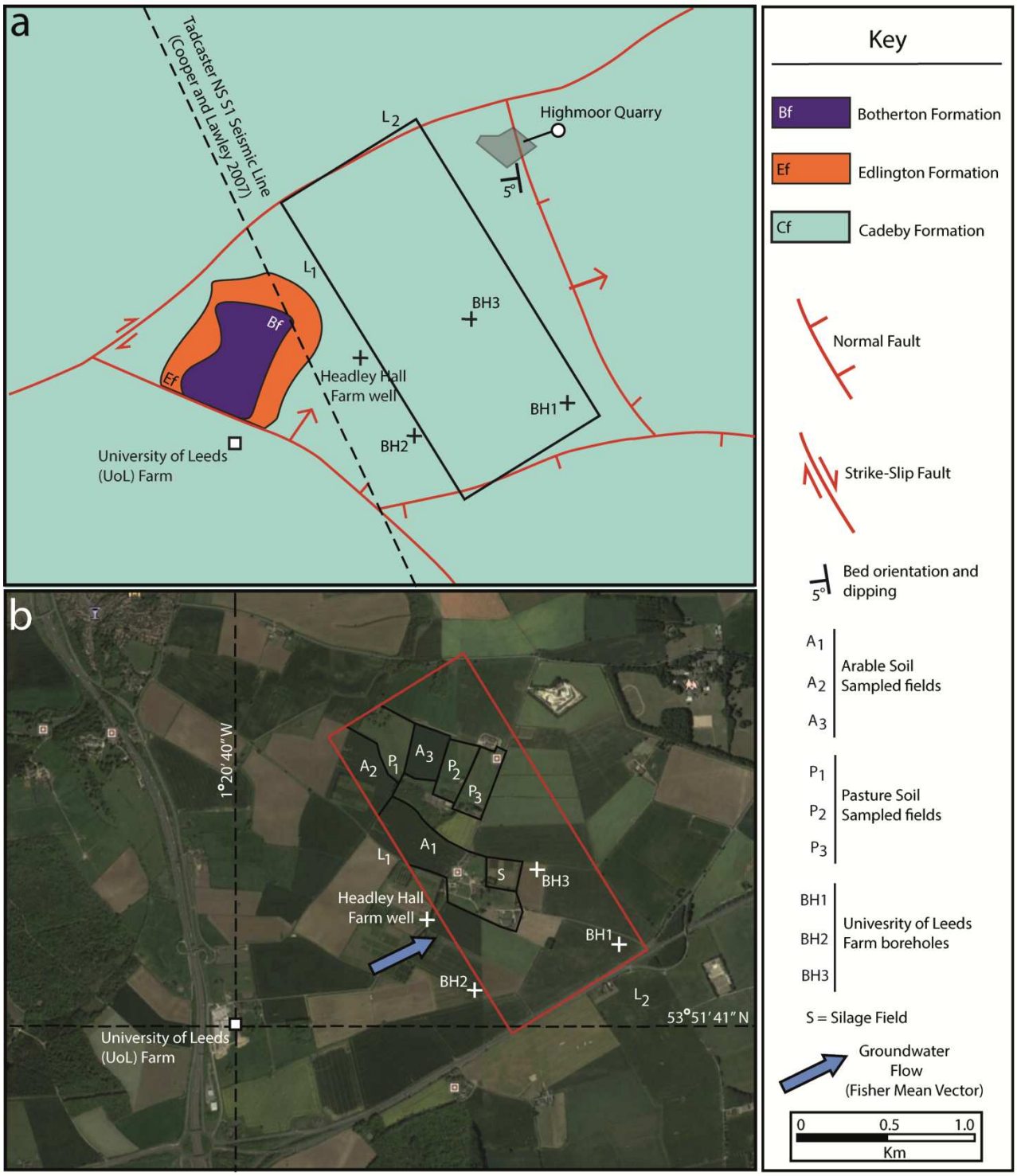

931

932 Fig. 2

933

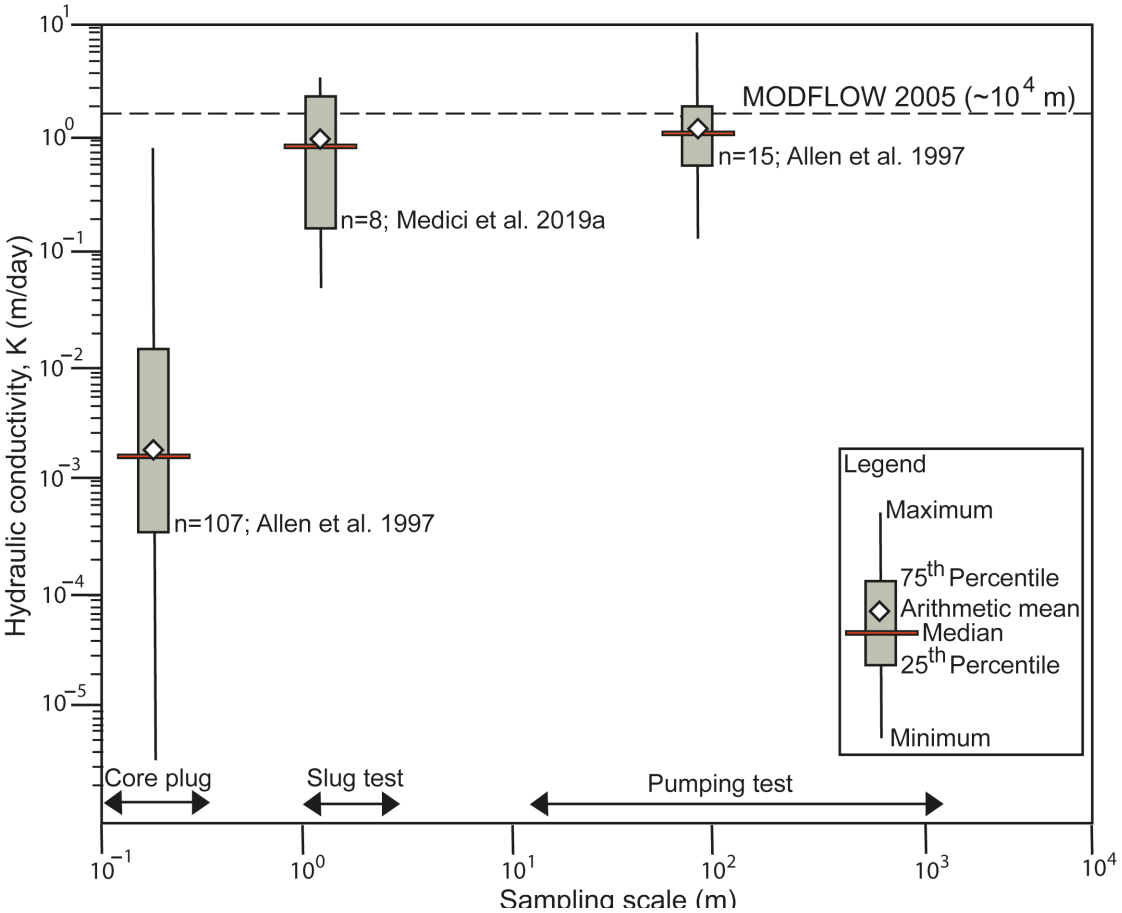

934

935 Fig. 3

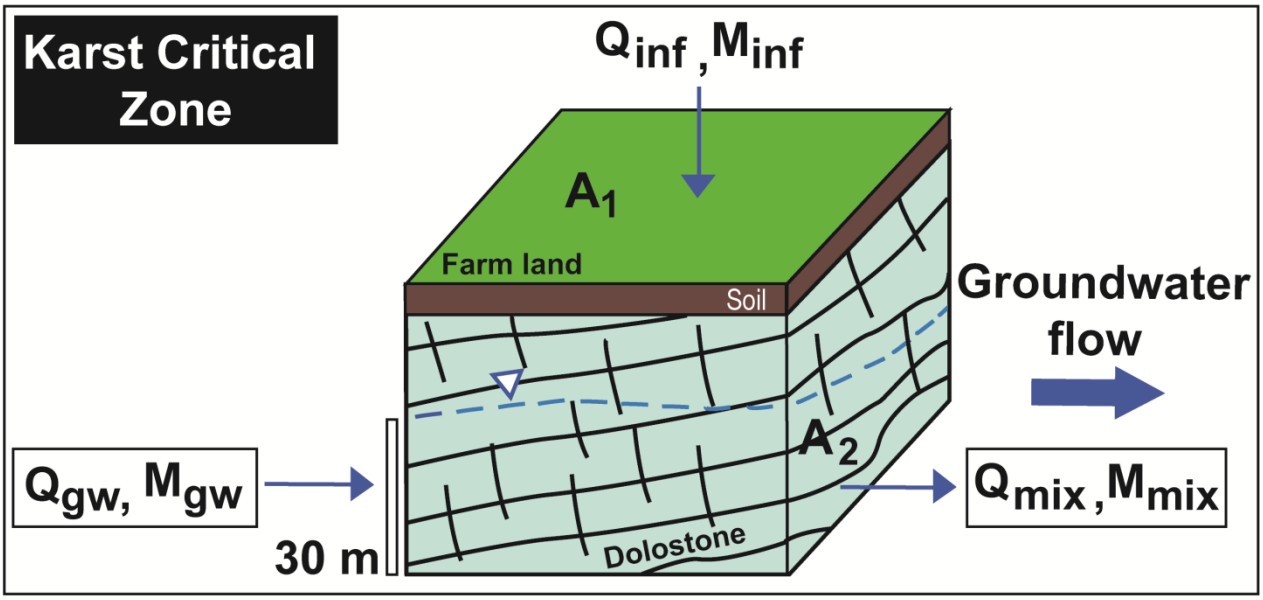

936

937 Fig. 4

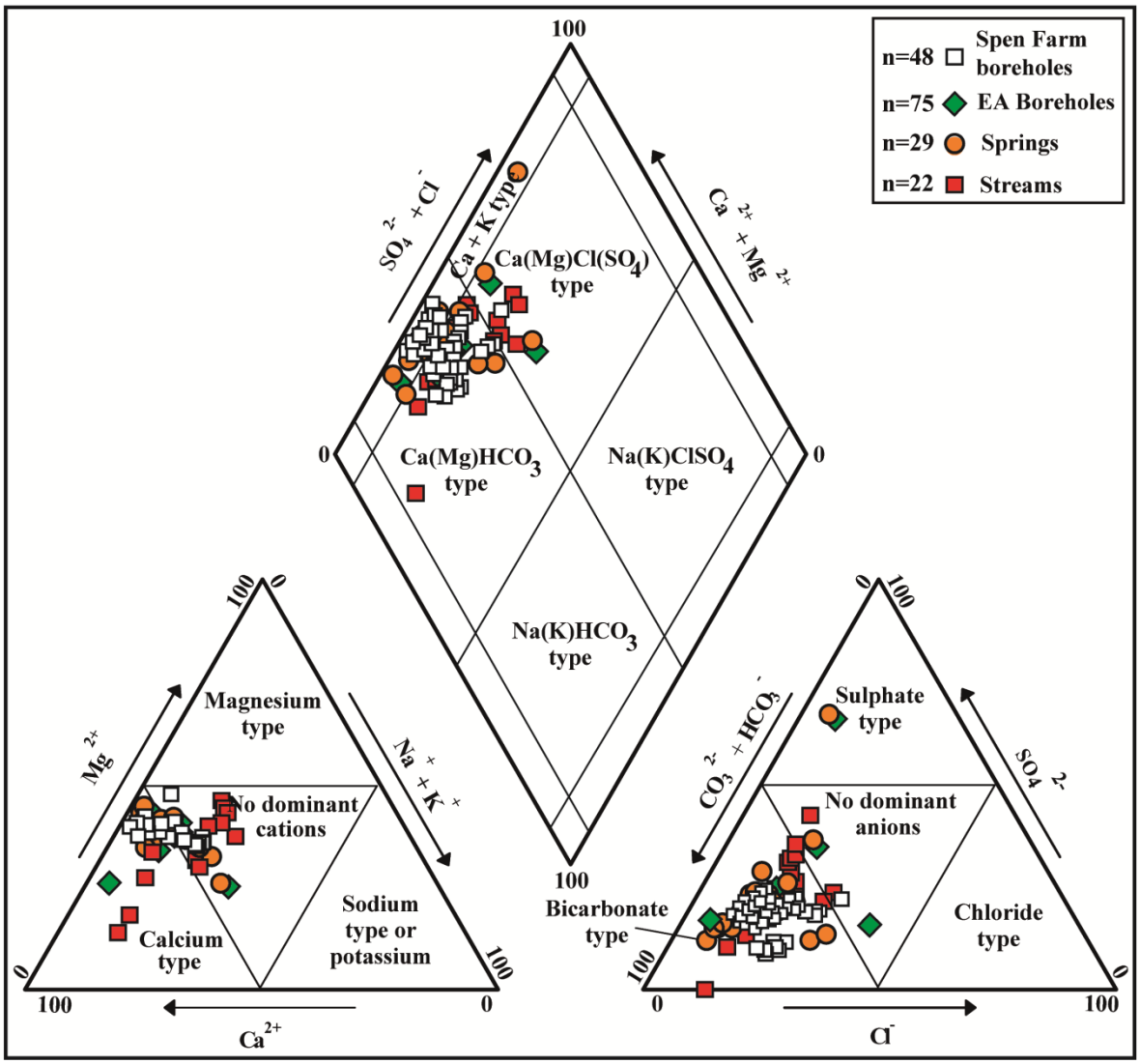

938

939 Fig. 5

940

941

942

943

944

945

946

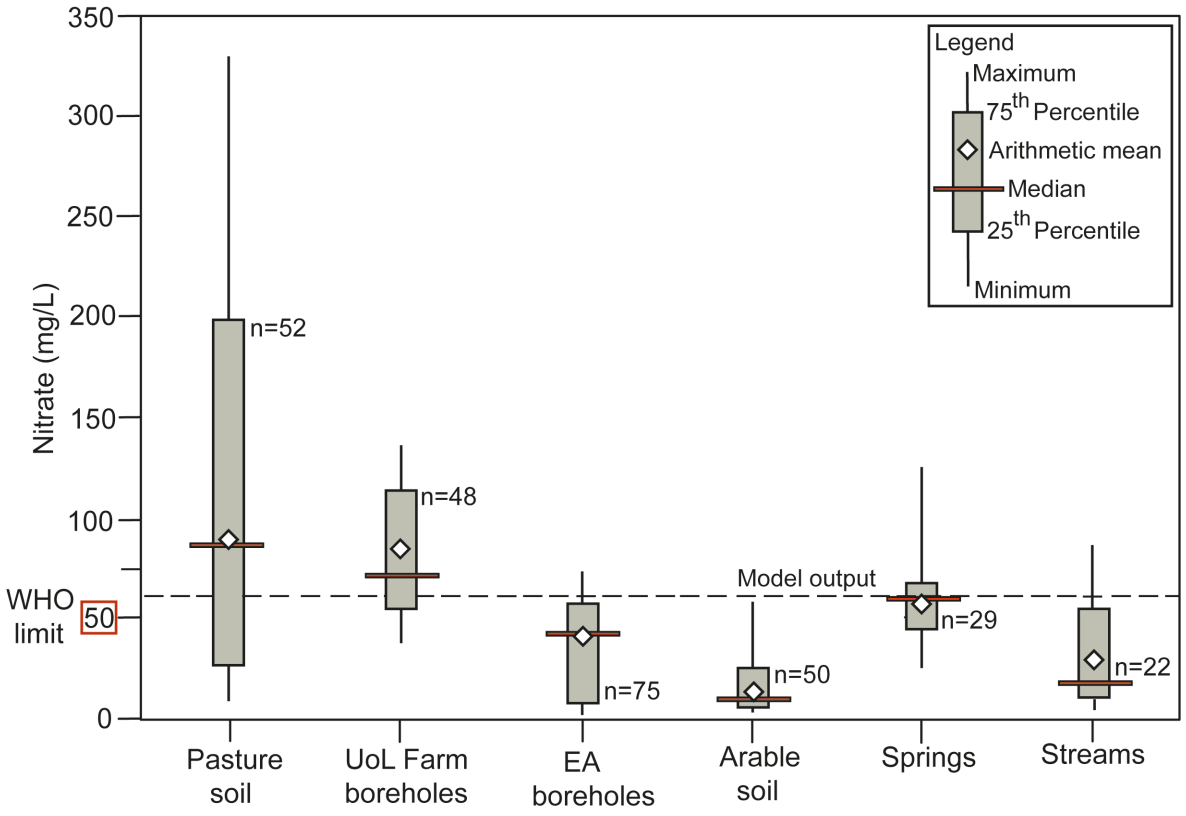
Legend
Maximum
75th Percentile
Arithmetic mean
Median
25th Percentile
Minimum
Nitrate (mg/L)
350
300
250
200
150
100
50
0
WHO limit
Model output
n=52
n=48
n=75
n=50
n=29
n=22
Pasture soil
UoL Farm boreholes
EA boreholes
Arable soil
Springs
Streams

Fig. 6

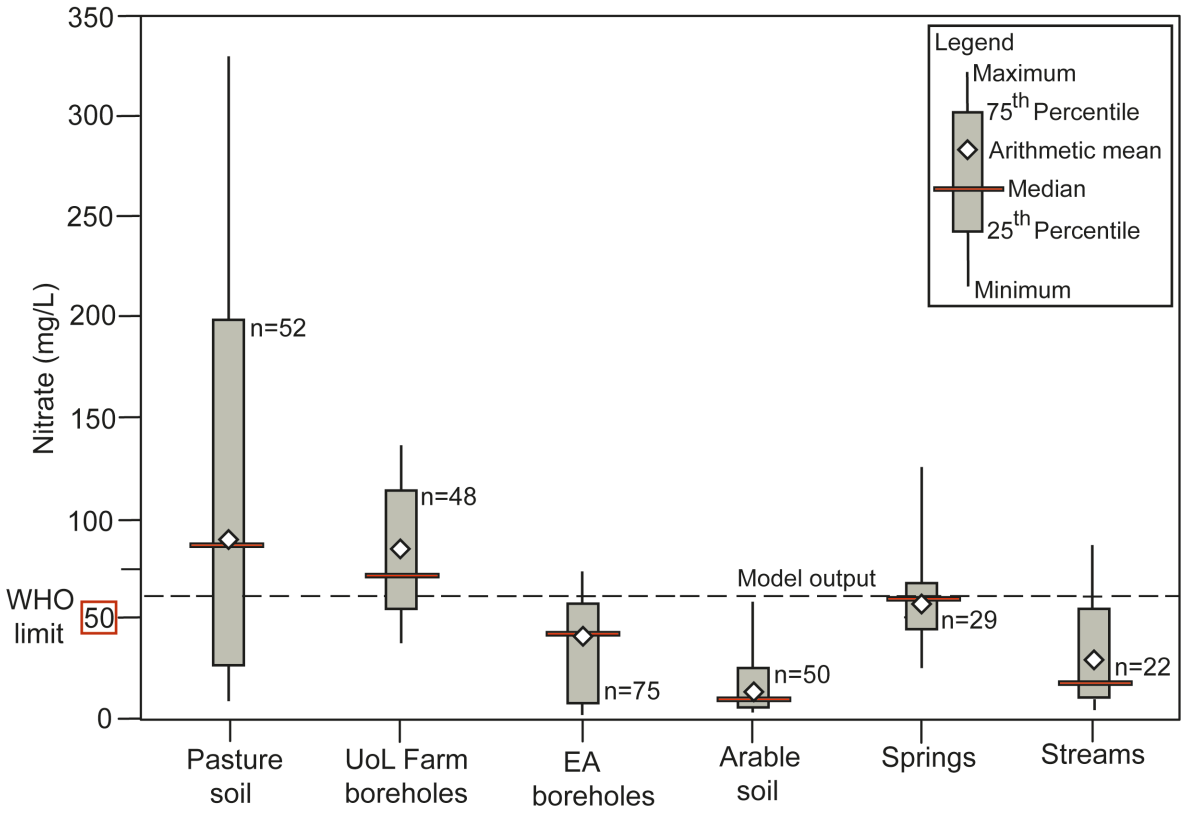
Legend
Maximum
75th Percentile
Arithmetic mean
Median
25th Percentile
Minimum
Nitrate (mg/L)
350
300
250
200
150
100
WHO limit
50
0
Model output
n=52
n=48
n=75
n=50
n=29
n=22
Pasture soil
UoL Farm boreholes
EA boreholes
Arable soil
Springs
Streams

959

960 Fig. 7

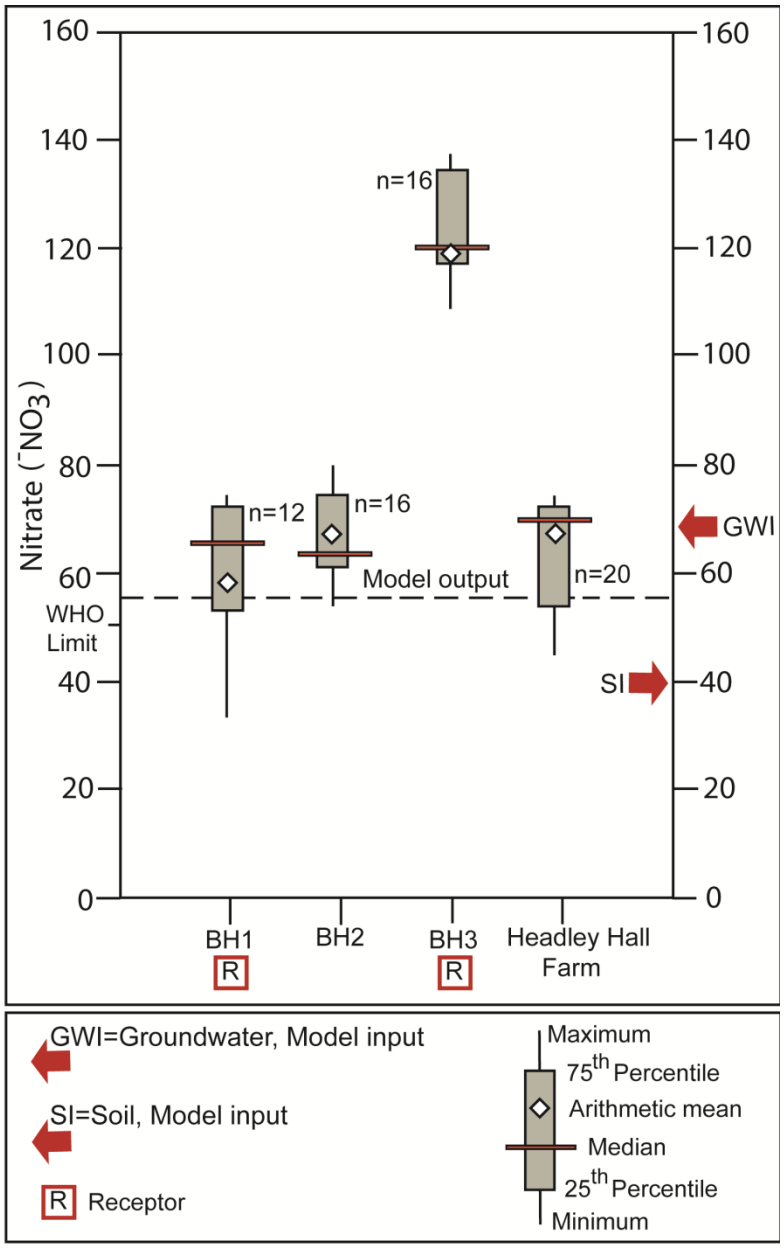

961

962 Fig. 8

963

964

965

966

967

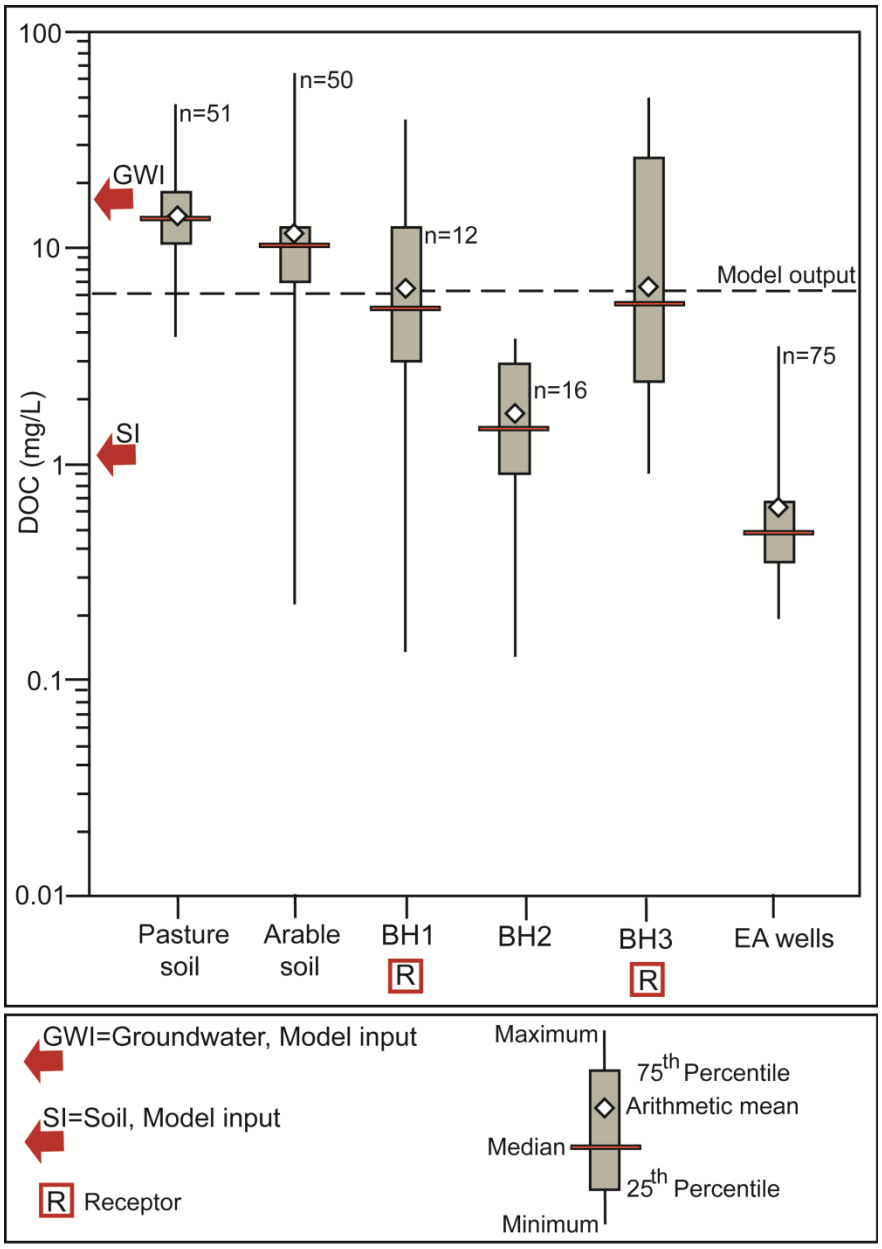

968

969 Fig. 9

970

971

972

973

974

975

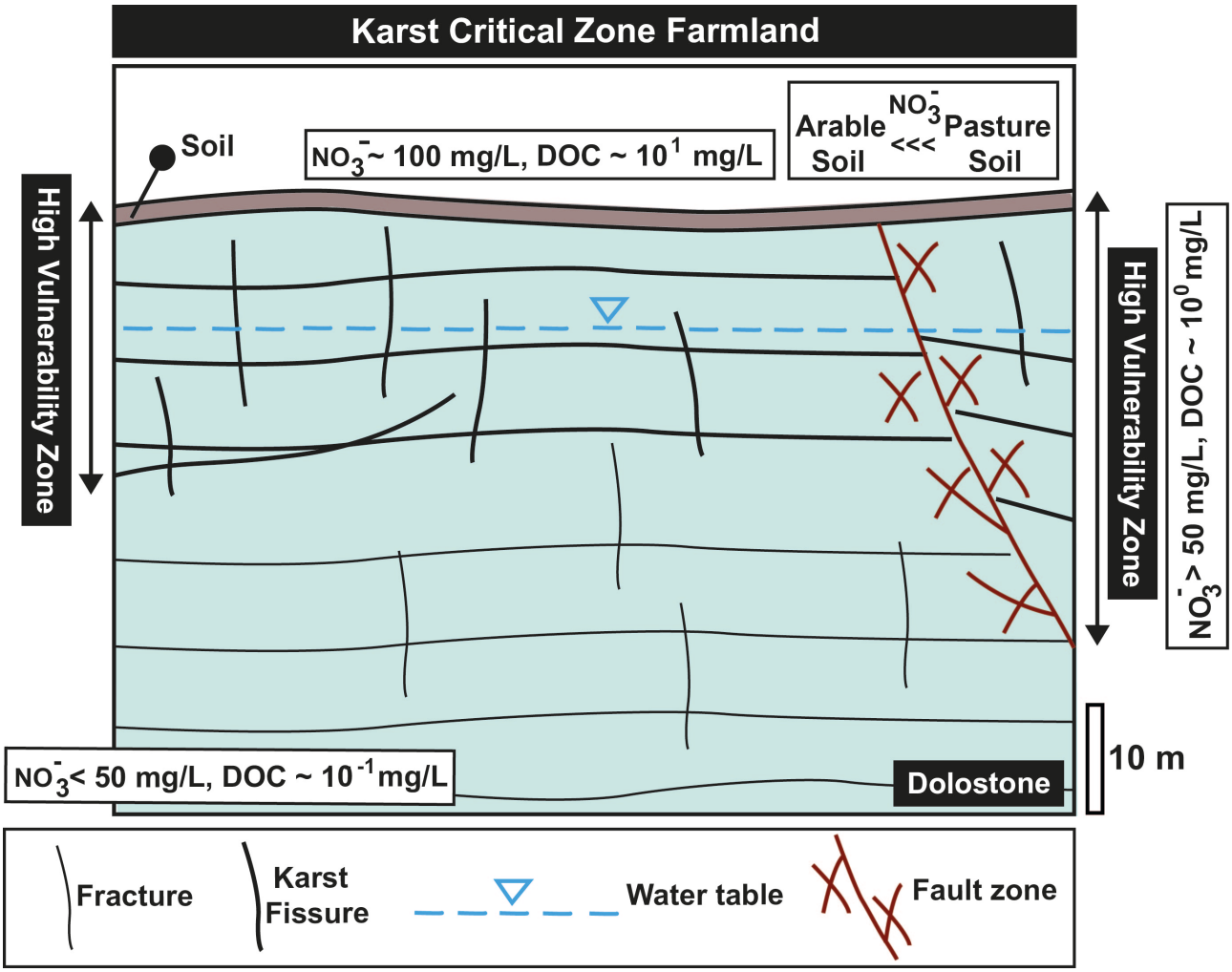
Karst Critical Zone Farmland
Soil
NO_3^-~ 100 mg/L, DOC ~ 10^1 mg/L
Arable Soil NO_3^- <<< Pasture Soil
High Vulnerability Zone
High Vulnerability Zone
NO_3^- > 50 mg/L, DOC ~ 10^0 mg/L
10 m
NO_3^-< 50 mg/L, DOC ~ 10^{-1} mg/L
Dolostone
Fracture
Karst Fissure
Water table
Fault zone

Fig. 10